NMR IN BIOMEDICINE
NMR Biomed. 2001;**14**:413–431
DOI:10.1002/nbm.733

Quantitative functional imaging of the brain: towards mapping neuronal activity by BOLD fMRI

Fahmeed Hyder,[1,2,5]* Ikuhiro Kida,[1] Kevin L. Behar,[3] Richard P. Kennan,[6] Paul K. Maciejewski[4] and Douglas L. Rothman[1,2,5]

[1]Departments of Diagnostic Radiology, Magnetic Resonance Center for Research in Metabolism and Physiology, Yale University, New Haven, CT, USA
[2]Department of Biomedical Engineering, Yale University, New Haven, CT, USA
[3]Department of Psychiatry, Yale University, New Haven, CT, USA
[4]Department of Internal Medicine, Magnetic Resonance Center for Research in Metabolism and Physiology, Yale University, New Haven, CT, USA
[5]Section of Bioimaging Sciences, Yale University School of Medicine, New Haven, CT, USA
[6]Department of Diagnostic Radiology, Albert Einstein College of Medicine, Bronx, NY, USA

Received 22 February 2001; Revised 22 August 2001; Accepted 22 August 2001

ABSTRACT: Quantitative magnetic resonance imaging (MRI) and spectroscopy (MRS) measurements of energy metabolism (i.e. cerebral metabolic rate of oxygen consumption, CMR_{O2}), blood circulation (i.e. cerebral blood flow, CBF, and volume, CBV), and functional MRI (fMRI) signal over a wide range of neuronal activity and pharmacological treatments are used to interpret the neurophysiologic basis of blood oxygenation level dependent (BOLD) image-contrast at 7 T in glutamatergic neurons of rat cerebral cortex. Multi-modal MRI and MRS measurements of CMR_{O2}, CBF, CBV and BOLD signal (both gradient-echo and spin-echo) are used to interpret the neuroenergetic basis of BOLD image-contrast. Since each parameter that can influence the BOLD image-contrast is measured quantitatively and separately, multi-modal measurements of changes in CMR_{O2}, CBF, CBV, BOLD fMRI signal allow calibration and validation of the BOLD image-contrast. Good agreement between changes in CMR_{O2} calculated from BOLD theory and measured by ^{13}C MRS, reveals that BOLD fMRI signal-changes at 7 T are closely linked with alterations in neuronal glucose oxidation, both for activation and deactivation paradigms. To determine the neurochemical basis of BOLD, pharmacological treatment with lamotrigine, which is a neuronal voltage-dependent Na^+ channel blocker and neurotransmitter glutamate release inhibitor, is used in a rat forepaw stimulation model. Attenuation of the functional changes in CBF and BOLD with lamotrigine reveals that the fMRI signal is associated with release of glutamate from neurons, which is consistent with a link between neurotransmitter cycling and energy metabolism. Comparisons of CMR_{O2} and CBF over a wide dynamic range of neuronal activity provide insight into the regulation of energy metabolism and oxygen delivery in the cerebral cortex. The current results reveal the energetic and physiologic components of the BOLD fMRI signal and indicate the required steps towards mapping neuronal activity quantitatively by fMRI at steady-state. Consequences of these results from rat brain for similar calibrated BOLD fMRI studies in the human brain are discussed.

KEYWORDS: oxygen; glucose; lactate; glutamate; glutamine; glycogen; neuron; astrocyte; cerebral activity; lamotrigine

**Correspondence to:* F. Hyder, 126 MRC, 330 Cedar Street, Yale University, New Haven, CT 06510, USA.
Email: fahmeed.hyder@yale.edu

Abbreviations used: BOLD, blood-oxygenation level dependent; CBF, cerebral blood flow; CBV, cerebral blood volume; CMR_{glc}, cerebral metabolic rate for glucose consumption; $CMR_{glc(ox)}$, cerebral metabolic rate for glucose oxidation; CMR_{O2}, cerebral metabolic rate for oxygen consumption; *D*, effective mass transfer coefficient for oxygen in the capillary bed; DANTE, delays alternating with nutations for tailored excitation; EPI, echo planar imaging; FLASH, fast low-angle shot; fMRI, functional MRI; ICED PEPSI, *in vivo* carbon edited detection with proton echo planar spectroscopic imaging; MRI, magnetic resonance imaging; MRS, magnetic resonance spectroscopy; OEF, oxygen extraction fraction; PET, positron emission tomography; POCE, ^1H observed ^{13}C editing; R_1, longitudinal relaxation rate of tissue water; R_2*, apparent tissue water relaxation rate; R_2, absolute tissue water relaxation rate; *TE*, echo time; *TIR*, inversion recovery time; *TR*, recycle time; V_{TCA}, tricarboxylic acid cycle flux; Y, blood oxygenation.

INTRODUCTION

Functional imaging of mammalian brain with magnetic resonance imaging (MRI) has become a popular modality in neuroscience,[1] but the exact relationship between the measured blood-oxygenation level dependent (BOLD) signal and the underlying neurophysiological parameters remains unclear. The BOLD functional MRI (fMRI) method allows detection of changes in blood oxygenation during a physiological stimulation with gradient-echo and spin-echo MRI.[2] The BOLD image-contrast relies on physiologically induced changes in the magnetic properties of blood (oxyhemoglobin is diamagnetic and deoxyhemoglobin is paramagnetic), where an increase

in the fractional BOLD fMRI signal-change ($\Delta S/S > 0$) is consistent with a drop in venous deoxyhemoglobin concentration.[1–5] At steady-state, $\Delta S/S$ is given by changes in neurophysiological parameters based on Fick's principle[3–5]

$$\Delta S/S = \acute{A}[(\Delta CBF/CBF - \Delta CMR_{O2}/CMR_{O2}) /(1 + \Delta CBF/CBF) - \Delta CBV/CBV] \quad (1)$$

where $\acute{A}$ is a measurable physiological and static magnetic field dependent constant and $\Delta CMR_{O2}/CMR_{O2}$, $\Delta CBF/CBF$ and $\Delta CBV/CBV$ are the changes in cerebral metabolic rate of oxygen consumption, cerebral blood flow and cerebral blood volume, respectively (see Appendix A). Of these physiological parameters, $\Delta CMR_{O2}/CMR_{O2}$ is the most relevant for studying functional brain activity,[6,7] because it is proportional to the change in energy consumption associated with changes in neuronal activity induced by the stimulation.

Methods which provide direct measurement of the rate of cortical energy utilization or production are considered as 'gold-standards' for detection of neuronal activity. In the autoradiography method[8] a ^{14}C labeled analog of glucose, 2-deoxyglucose, is infused into the blood stream in trace amounts. The radioactive analog crosses the blood–brain barrier and is phosphorylated much like glucose. Since the ^{14}C labeled phosphate cannot be metabolized further, its concentration is proportional to the cerebral metabolic rate of glucose consumption (CMR_{glc}). The positron emission tomography (PET) fluoro-deoxyglucose method uses similar principles to deoxyglucose autoradiography but measures the distribution of fluoro-deoxyglucose-6-phosphate. *In vivo* ^{13}C magnetic resonance spectroscopy (MRS) detection of infused ^{13}C labeled glucose, a stable isotope, can provide important information on brain energy metabolism.[6,7] The flow of ^{13}C label from glucose to glutamate can be used to calculate the tri-carboxylic acid cycle flux (V_{TCA}), cerebral metabolic rates of glucose oxidation ($CMR_{glc(ox)}$) which is proportional to CMR_{O2}. Under normal physiological conditions, glucose is the major energy substrate in the mammalian cortex and it is metabolized[9] either in the presence of oxygen (via glucose oxidation generating 32–34 ATP/glucose, CO_2, and H_2O) or absence of oxygen (via glycolysis and/or glycogen shunt generating 1–2 ATP/glucose and lactate). BOLD fMRI has become the method of choice for human brain mapping, because of its high spatial and (relative to PET) temporal resolution, as well as its being non-hazardous and non-invasive. As shown in eqn (1), in principle the BOLD fMRI signal, in combination with measurements of CBF and CBV, can be used to map regional changes in CMR_{O2} (or $CMR_{glc(ox)}$). Such quantitative BOLD fMRI approaches which allow maps of regional energy metabolism with the spatial resolution of MRI, would pay great dividends towards mapping of neuronal activity in the intact human brain.

In this paper, we explore the neurophysiological basis of BOLD fMRI at 7 T in rat brain for the purpose of neuronal activity mapping at steady-state. We present multi-modal measurements of changes in CMR_{O2}, CBF, CBV, and BOLD signal in rat cerebral cortex at 7 T over a wide range of neuronal activity and pharmacological treatments. This approach differs from others in the field[10–12] because each parameter in eqn (1) that influences the image-contrast is measured independently in rat cerebral cortex. Furthermore this approach allows validation of BOLD image-contrast, because the *predicted* changes in CMR_{O2} based on BOLD theory [rearrangement of eqn (1)] can be compared with the independently *measured* changes in CMR_{O2} based on *in vivo* ^{13}C MRS.[6] The method of indirect ^{13}C MRS detection (i.e. using ^{1}H instead of ^{13}C) for $CMR_{glc(ox)}$ and CMR_{O2} measurements is discussed. Insights into energy metabolism and oxygen delivery of glutamatergic neurons are gained from comparisons of CMR_{O2} and CBF over a wide range of activity.

MATERIAL AND METHODS

Animal preparation

Adult, male, Sprague–Dawley rats (110–280 g; fasted >16 h) were tracheotomized under halothane (0.7–1.2%) anesthesia and artificially ventilated (70% N_2O/30% O_2). A femoral artery was cannulated for continuous mean arterial blood pressure monitoring and periodic sampling for measurement of blood gases, pH, pressure, and glucose. Femoral veins were cannulated for intravenous (i.v.) infusions of nicotine hydrogen tartrate, iron oxide contrast agent (AMI-227; Advanced Magnetics Inc., Cambridge, MA), and/or D-[1-^{13}C] or [1,6-^{13}C]glucose (99 atom %; Cambridge Isotopes, Andover, MA). Intraperitoneal (i.p.) lines were inserted for administration of anesthetic, paralyzing, and/or pharmacological agents. The scalp was retracted and a layer of Saran Wrap was placed over the skull. The rat was placed prone in a cradle and covered with a water blanket to maintain body temperature (~37 °C). Halothane was discontinued after the positioning and anesthesia was maintained throughout with either morphine sulfate or α-chloralose and paralyzed with D-tubocurarine chloride (initial 0.5 mg/kg; supplemental 0.25 mg/kg/30 min; i.p.). The head was secured with a bite-bar and tightly fixed by foam cushions on either side of the head. The center of the radio-frequency surface-coil was placed above the bregma.

General MRI and MRS experimental setups

All *in vivo* MRI and MRS data were obtained on a modified 7 T Bruker Biospec or AVANCE horizontal-

bore spectrometer (Bruker Instruments, Billerica, MA) operating at 300.6 and 75.5 MHz for ^{1}H and ^{13}C, respectively. Indirect ^{13}C MRS [i.e. ^{1}H observed ^{13}C editing (POCE) experiments] and all MRI data were acquired with an ^{1}H resonator radio-frequency transmit (8 cm diameter) for homogeneous transmission and a ^{1}H radio-frequency surface-coil receiver (10 mm diameter) for local reception. This radio-frequency coil arrangement[13] allows better shimming, minimizes sensitivity loss in the receiver coil, and results in high signal-to-noise ratio for ^{1}H. A concentric ^{13}C radio-frequency surface-coil (20 mm diameter) was used for transmission and decoupling in the POCE experiments (for CMR_{O2} measurements; see below). High signal-to-noise ratio ^{1}H spectra with ^{13}C composite pulse decoupling[14] were acquired every ~5 min. Direct ^{13}C MRS data were acquired with a dual surface radio-frequency coil system consisting of a circular ^{13}C coil (10 mm diameter) for transmission and a butterfly ^{1}H coil for decoupling where the ^{13}C radio-frequency excitation pulse was optimized for cortical signal detection.[15] High signal-to-noise ratio ^{13}C spectra with nuclear Overhauser enhancement and ^{1}H broadband decoupling[14] were acquired every ~10 min.

High-resolution, multi-slice, fast low-angle shot (FLASH) coronally oriented anatomical images [weighted by longitudinal (R_1) relaxation rate of tissue water] were acquired [image matrix = 128 × 128; in-plane resolution = 156 × 156 μm^2; slice thickness = 500 μm; repetition time (TR) = 250 ms; echo time (TE) = 20 ms; inversion recovery time (TIR) = 300 ms]. These images provided coordinates for the placement of a 7.5 × 1.6 × 4.0 mm^3 region of interest for the POCE experiments.[16,17] The static magnetic field homogeneity of a 8 × 2 × 5 mm^3 volume in the sensorimotor cortex was optimized. Details of the localized POCE pulse sequence have been described earlier.[16–18] Chemical shift imaging ^{13}C turnover data were obtained using *in vivo* carbon edited detection with proton echo planar spectroscopic imaging (ICED PEPSI), which combines echo-planar imaging (EPI) with ^{13}C-^{1}H *J*-editing and semi-selective water suppression of POCE.[19,20] Multi-modal MRI data were acquired with EPI using sequential sampling.[21] The distortions in EPI associated with spin-echo were minimal[22] because the total acquisition time of all echoes was 20.48 ms. All multi-parametric MRI measurements were made with coronally oriented multi-slice EPI acquisitions with 1 mm slice separation (image matrix = 32 × 32 or 32 × 64; in-plane resolution = 320 × 320 or 430 × 430 μm^2; slice thickness = 1000 μm; $TR \geq 5000$ ms). A sinc pulse was used for slice excitation and an adiabatic fast passage hyperbolic secant pulse was used for slice refocusing as well as inversions. All data were acquired under steady-state conditions.

Protocols and methods for BOLD calibration studies

Multi-modal measurements were divided into five treatment groups, but prior to the start of each MRI and MRS protocol, a delays alternating with nutations for tailored excitation (DANTE) method was used (see below) for estimation of static magnetic field distortion in the region of interest.[23,24] Values of BOLD fMRI signal (both gradient-echo and spin-echo), CBF and CBV were obtained (by averaging) from the same region of interest (48 or 8 μl) as the CMR_{O2} measurements were made from.[23,24]

The rats in group α ('control I') were anesthetized with morphine sulfate (initial 50 mg/kg; supplemental 30 mg/kg/30 min; i.p.), where the rats in groups β and γ received in addition sodium pentobarbital (initial 45 mg/kg initial; supplemental 10 mg/kg/30 min; i.p.) and nicotine hydrogen tartrate (dose of 4 mg/kg; rate of 16.7 μl/min; i.v.), respectively.[13,23,24] The rats in group δ ('control II') were anesthetized with α-chloralose (initial 80 mg/kg; supplemental 20 mg/kg/30 min; i.p.), where the rats in group ε received electrical stimulation (2–3 V square pulses of 0.3 ms duration at 3 Hz; Harvard Apparatus Limited, Kent, MA) of the forepaw[13,25] using a pair of thin copper electrodes.

For each rat in group α, BOLD fMRI signal (both gradient-echo and spin-echo), CMR_{O2}, $CMR_{glc(ox)}$ and CBF were measured together under basal conditions of morphine/nitrous oxide anesthesia. For each rat in group β, the BOLD fMRI signal (both gradient-echo and spin-echo) and CBF were measured before pentobarbital administration under basal conditions, then BOLD fMRI signal (both gradient-echo and spin-echo), CMR_{O2}, $CMR_{glc(ox)}$ and CBF were measured together after pentobarbital administration. For each rat in group γ, the BOLD fMRI signal (both gradient-echo and spin-echo) and CBF were measured before nicotine administration under basal conditions, then BOLD fMRI signal (both gradient-echo and spin-echo), CMR_{O2}, $CMR_{glc(ox)}$ and CBF were measured together after nicotine administration. In two cases, each group received an anesthetic dose of α-chloralose (initial 80 mg/kg; supplemental 20 mg/kg/30 min; i.p.) balanced with nitrous oxide either alone (group δ) or in combination with forepaw stimulation (group ε) to increase focal activity in the sensorimotor region.[16] For each rat in Groups δ and ε, BOLD fMRI signal (both gradient-echo and spin-echo), CMR_{O2}, $CMR_{glc(ox)}$ and CBF were measured at rest ('control II') and during stimulation of both forepaws. For relative CBV measurements separate groups of rats were divided into the same five treatment groups described above (i.e. groups α–ε) and BOLD fMRI signal (both gradient-echo and spin-echo) were mapped with AMI-227 for each condition.

Single-exponential fits of the multi TE (ranging from 10 to 80 ms) gradient-echo and spin-echo MRI data were

used to obtain transverse relaxation rates of tissue water, R_2*(obs) and R_2(obs), respectively. We used the following relaxation rate term to describe the BOLD fMRI signal (see Appendix A)

$$R_2'(Y) = R_2^*(\text{obs}) - R_2(\text{obs}) - R_2^*(\Delta B_o) \qquad (2)$$

where R_2*(ΔB_o) is the relaxation component of tissue water relaxation rate attributed to macroscopic distortions of static magnetic field (ΔB_o), and $R_2'(Y)$ is the reversible relaxation component tissue water relaxation rate due to blood oxygenation effects. The R_2*(ΔB_o) component within the region of interest was estimated by an MRI sequence[26] with a double spin tagging sequence using DANTE pulses as described previously.[23,24] The BOLD fMRI signal-change at steady-state in eqn (1) is also given by

$$\Delta S/S = \exp(-\Delta R_2'(Y) \times TE) - 1 \qquad (3)$$

where TE is 25 ms and $\Delta R_2'(Y)$ is the change in the relaxation rate term described by eqn (2). The advantage of this definition for the BOLD signal is that the common and unknown terms between R_2*(obs) and R_2(obs) are subtracted away[24] leaving only the pure oxygenation term which can be described as[1–5]

$$R_2'(Y) = C\nu_{\max}(1 - Y)b \text{ Hct} \qquad (4)$$

where C is a BOLD proportionality constant, $\nu_{\max}$ is the magnetic field-dependent deoxyhemoglobin susceptibility frequency shift, b is the blood volume fraction, $(1 - Y)$ is the blood deoxygenation, and Hct is the blood hematocrit (see Appendix A for other details).

The relative changes in CBV from the baseline to lower or higher conditions were measured by administration of a high susceptibility MRI contrast agent to enhance blood volume induced changes in R_2(obs) or R_2*(obs). The blood volume susceptibility was raised through serial injections (2 mg/kg/0.9 ml bolus) of an iron oxide contrast agent AMI-227 which remains in the intravascular space for several hours.[27] The relative changes in CBV were calculated by ΔCBV/CBV $= (\Delta R^{w} - \Delta R^{w/o})/(R^{w} - R^{w/o})$, where R^{w} and $R^{w/o}$ are the rates at the reference conditions with and without agents, respectively, and ΔR^{w} and $\Delta R^{w/o}$ are the rate differences as a consequence of transition from baseline to lower or higher conditions with and without agents, respectively. Details of relative experimental errors have been described earlier.[24,27,28]

The absolute CBF maps were obtained using the spin-echo slice selective and non-slice selective inversion-recovery weighted EPI data.[13,29] A single-exponential recovery fit to the multi TIR data (ranging from 200 to 2200 ms) was used to create R_1 maps for the slice selective (R_{1s}) and non-slice selective (R_{1n}) images. The longitudinal relaxation rate of arterial blood water (R_{1b}) was determined (0.50 ± 0.03 s^{-1}) from high-resolution CBF data,[13] and the brain–blood partition coefficient for water (λ) was assumed to be 0.95 ml/g.[29] Absolute perfusion was calculated by CBF = 60 λ ($R_{1app} - R_{1b}$), where R_{1app} is the apparent relaxation rate given by $[R_{1b} + (R_{1s} - R_{1n})/(1 + \Gamma)]$ and Γ is a small correction factor, given by $3/4(1 - R_{1b}/R_{1n})$, which accounts for the difference between longitudinal relaxation rates of tissue water and arterial blood water.[29] Details of the associ-

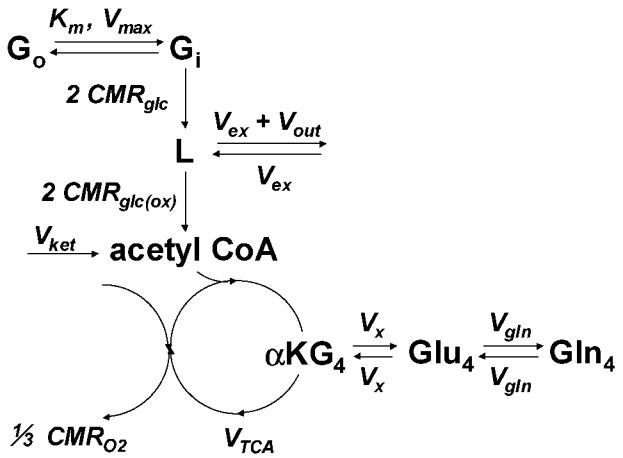

Figure 1. Schematic representation of the metabolic model at isotopic mass balance.[16,17,31,32] The [1-^{13}C] or [1,6-^{13}C]glucose in plasma (G_o) and brain (G_i) exchange via Michaelis–Menten kinetic parameters K_m (half-saturation concentration for transport) and V_{max} (maximum transport rate), where K_m ranges from 10 to 15 mM and V_{max}/CMR_{glc} ranges from 5 to 25. Under most conditions the calculated V_{TCA} is insensitive to the reported range of these parameters.[16] The ^{13}C label flows at the rate $2 \times CMR_{glc}$ through the glycolytic intermediates (negligible concentrations) and arrives at C3-pyruvate and C3-lactate, represented by L (1.5 μmol/g). Two sources of ^{12}C entrance into the tricarboxylic acid cycle are exchange of blood–brain pyruvate and lactate pool (V_{ex}) and the ketone body flux (V_{ket}), both of which dilute the ^{13}C fractional enrichment of intermediates in the tri-carboxylic acid cycle. The efflux at L, V_{out}, causes some ^{13}C label to be lost to blood. The ^{13}C label enters the acetyl CoA pool at a rate of $2 \times CMR_{glc(ox)}$ prior to its entry into the tri-carboxylic acid cycle. The ^{13}C label enters the tricarboxylic acid cycle and labels C4-α-ketoglutarate, αKG_4, and C4-glutamate (12.0 μmol/g), Glu_4. These two pools are in very rapid isotopic exchange, V_x, where $V_x/V_{TCA} \gg 1$.[31,32] There is an exchange between C4-glutamate and C4-glutamine (6.2 μmol/g), Gln_4, at a rate of V_{gln} (where V_{gln}/V_{TCA} ranges from 0.25 to 1.[16]). V_{TCA} is approximately equal to $1/3CMR_{O2}$ (see Appendix B for other details). In the first pass of the tri-carboxylic acid cycle the ^{13}C label arrives at C4-glutamate (i.e. Glu_4), which reflects pyruvate dehydrogenase activity (in the neuron), whereas in the second and subsequent passes of the cycle the ^{13}C label arrives at C2- and C3-glutamate. However, some pyruvate carboxylase activity (in the astrocyte) could lead to labeling of C3-oxaloacetate which would subsequently lead to labeling of C3-glutamate also. Since each metabolic modeling was carried out with the ^{13}C isotopic turnover rate of C4-glutamate, which represents labeling from C1,6 or C1-glucose in the first turn of the tri-carboxylic acid cycle and pyruvate dehydrogenase activity in the neuron, the pyruvate carboxylase activity in the astrocyte will not modify our results of V_{TCA} estimates

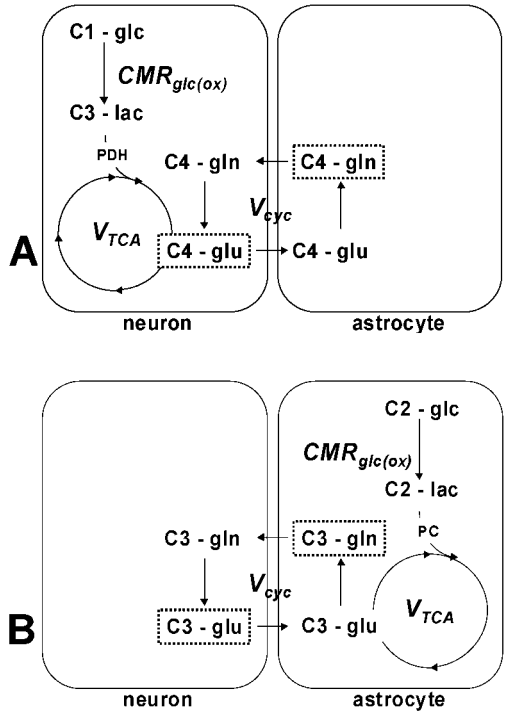

Figure 2. (A) In the [1-^{13}C]glucose experiment, the ^{13}C label flows from C1-glucose to C3-pyruvate and C3-lactate, and through the tri-carboxylic acid cycle intermediates, into C4-glutamate due to fast isotopic exchange between C4-glutamate and C4-α-ketoglutarate. C4-glutamate in the neuron serves as a precursor for C4-glutamine in the astrocyte. Since C4-glutamine labeling lags behind C4-glutamate under these situations, the [1-^{13}C]glucose experiment mainly reflects neuronal pyruvate dehydrogenase (PDH) activity. (B) In the [2-^{13}C]glucose experiment, the ^{13}C label flows from C2-glucose to C2-pyruvate and C2-lactate and enters the tri-carboxylic acid cycle resulting in C5-glutamate labeling. However, this ^{13}C label is lost as $^{13}CO_2$ in the first turn of the tri-carboxylic acid cycle via the pyruvate dehydrogenase reaction in the neuron. However, ^{13}C label can also lead to consequent C3 labeling in intermediates of the tri-carboxylic acid cycle via the pyruvate carboxylase (PC) reaction in the astrocyte. Thus in the [2-^{13}C]glucose experiment C3-glutamine labeling is detected prior to C3-glutamate under steady-state conditions, which indicates that the [2-^{13}C]glucose experiment mainly reflects astrocytic pyruvate carboxylase activity. In both of these experiments the time lag observed between labeling of glutamate and glutamine can be modeled[7] to determine glutamate-glutamine neurotransmitter flux (V_{cyc})

ated experimental errors have been described previously.[13,29,30]

Details of the direct and indirect ^{13}C MRS experiments for measurements of V_{TCA} have been described.[6,7,13,16,17,31,32] Time courses of C4-glutamate labeling were normalized to the ^{13}C fractional enrichment of C1,6 or C1-glucose. A set of coupled differential equations were used to describe the model (Fig. 1; Appendix B), and an iterative method was used to fit the model to the C4-glutamate turnover data to yield V_{TCA} estimates. Inflows from other unlabeled substrates (e.g. ketone bodies, V_{ket}; pyruvate and lactate blood–brain exchange, V_{ex}) can dilute the acetyl CoA pool. Comparison of the measured ^{13}C fractional enrichment of C4-glutamate and C1,6 or C1-glucose permits determination of the total dilution of the acetyl CoA pool, V_{dil} (see Appendix B). The values of CMR_{O2} and $CMR_{glc(ox)}$ were determined by

$$CMR_{glc(ox)} = 1/2(V_{TCA} - V_{dil}) \quad (5)$$

$$CMR_{O2} = 3(V_{TCA} - 3/4V_{dil}) \quad (6)$$

Equations (5) and (6) describe metabolic fluxes derived from a [1-^{13}C] or [1,6-^{13}C]glucose experiment which primarily reflects flows through pyruvate dehydrogenase which is localized in the neuron, whereas a [2-^{13}C]glucose experiment reflects flows through pyruvate carboxylase which is localized in the astrocyte (see Fig. 2; 'Measurements of neuroenergetics using ^{13}C MRS' in Discussion). Partial-volume corrected CMR_{O2} and $CMR_{glc(ox)}$ were obtained for the forepaw stimulation data (group ε) as previously described[17] using the relationship of $\omega(\text{activated}) = [\omega(\text{observed}) - (1-f) \times \omega(\text{rest})]/f$, where f represents the fraction of activated tissue in the compartment using the activated CBF maps thresholded at the resting CBF value, and ω represents the metabolic rates $CMR_{glc(ox)}$ and/or CMR_{O2}. The modeling parameters which have secondary effects on V_{TCA}, CMR_{O2} and $CMR_{glc(ox)}$ have been described previously[6,7,13,16,17,31,32] (Fig. 1; Appendix B).

Calibration of the BOLD fMRI signal

The determination of $\Delta CMR_{O2}/CMR_{O2}$ from measurements of $\Delta S/S$ requires that the values of $\acute{A}$, ΔCBF/CBF and ΔCBV/CBV be measured. The majority of studies attempting this calibration have measured just ΔCBF/CBF, assumed ΔCBV/CBV, and determined $\acute{A}$ either from theoretical calculations or by measuring $\Delta S/S$ and ΔCBF/CBF during transient manipulations of blood CO_2 levels. Our approach differs in that we have directly measured, over a wide range of brain activity induced by variable anesthesia and functional activation, the relative differences of fractional changes in four parameters [eqn (1)]; $\Delta S/S$ (measured by MRI), ΔCBF/CBF (measured by MRI), ΔCBV/CBV (measured by MRI), and $\Delta CMR_{O2}/CMR_{O2}$ (measured by MRS). The determination of the normalization constant $\acute{A}$ was obtained by dividing both sides of eqn (1) by ΔCBF/CBF and rearranging to result in

$$\acute{A} = \theta/[(1-\Psi)/(1+\Delta\text{CBF/CBF}) - \Lambda] \quad (7)$$

where $\theta = (\Delta S/S)/(\Delta\text{CBF/CBF})$, $\Psi = (\Delta CMR_{O2}/CMR_{O2})/(\Delta\text{CBF/CBF})$, and $\Lambda = (\Delta\text{CBV/CBV})/(\Delta\text{CBF/CBF})$. It should be emphasized that, while the CBV method in this

study measures changes in total plasma vascular space, the BOLD measurement is sensitive to venous blood volume compartment. Since each term in eqns (1) and (7) was measured over a wide range of neuronal activity at 7 T in rat cortex, the parameter $\acute{A}$ was determined purely from experimental data. The normalized approach to determination of $\acute{A}$ [eqn (7)] avoids biases towards arbitrary values of $\Delta S/S$, which has potential to be affected by the resting baseline value.[33]

Validation of the calibrated BOLD fMRI signal by comparison with MRS

In order to calculate $\Delta CMR_{O2}/CMR_{O2}$ from multi-modal MRI measurements, eqn (1) was rearranged to

$$\Delta CMR_{O2}/CMR_{O2} = \Delta CBF/CBF - [(\Delta S/S)/\acute{A} + \Delta CBV/CBV](1 + \Delta CBF/CBF) \quad (8)$$

which can be further simplified by the relationship between CBV and CBF[34]

$$\Delta CBV/CBV = (1 + \Delta CBF/CBF)^{\varphi} - 1 \quad (9)$$

to allow calculation of $\Delta CMR_{O2}/CMR_{O2}$ from only BOLD and CBF measurements (by MRI only)

$$\Delta CMR_{O2}/CMR_{O2} = \Delta CBF/CBF - [(\Delta S/S)/\acute{A} + (1 + \Delta CBF/CBF)^{\varphi} - 1](1 + \Delta CBF/CBF) \quad (10)$$

The value of $\acute{A}$ was calculated from the calibration curve described above [eqn (7)]. Although the relationship expressed by eqn (10) is similar to others,[10–12] we have sought to measure each parameter on the right-hand side of eqn (8) to predict $\Delta CMR_{O2}/CMR_{O2}$.[23,24] Comparison of predicted [by eqn (8) using MRI data] and measured (by POCE using MRS data) values of $\Delta CMR_{O2}/CMR_{O2}$ under conditions of variable anesthesia and sensory stimulation allowed validation of this method

$$\Delta CMR_{O2}/CMR_{O2}[\text{predicted by eqn}(8)] = m[\Delta CMR_{O2}/CMR_{O2}(\text{measured by POCE})] \quad (11)$$

where m approaches unity if the *predicted* and *measured* values $\Delta CMR_{O2}/CMR_{O2}$ are in agreement. This validation is essentially a test of how well a single value of $\acute{A}$ (with TE ranging from 20 to 34 ms) is able to normalize the BOLD signal over a large range of activity.

Neurochemical basis of BOLD fMRI

Details of this experiment have been described previously.[35] In a separate group of α-chloralose anesthetized rats, BOLD and CBF maps were obtained during rest and forepaw stimulation (see above). A BOLD fMRI experiment with FLASH consisted of a pre-stimulation rest period followed by forepaw stimulation and a post-stimulation rest period. The interval between successive scans was ~10 min. Three control BOLD experiments were completed before injection of lamotrigine (6-[2,3-dichlorophenyl]-1,2,4-triazine-3,5-diamine; 25 mg/kg; i.p.), which is a neuronal voltage-dependent Na^+ channel blocker and neurotransmitter glutamate release inhibitor. The BOLD and CBF experiments were performed approximately every 15 min, before and after lamotrigine treatment.

High-resolution CMR_{O2} mapping by calibrated BOLD fMRI

In another group of α-chloralose anesthetized rats (initial 40 mg/kg; supplemental 20 mg/kg/30 min; i.p.), an MRI method[36] was used that allows the measurement of changes in BOLD signal (both gradient-echo and spin-echo), CBF and CBV in a rapid manner (~1 min). We refer to the method as blood oxygenation level dependent exponential decays adjusted for flow attenuated inversion recovery (BOLDED AFFAIR). The method allows interleaved measurements of both transverse (R_2 and R_2*) and longitudinal (R_1) relaxation rates of tissue water in conjunction with pulsed arterial spin labeling. The image-contrasts are intrinsically oxygenation and flow weighted but each contrast is made quantitative by two *TE* and *TIR* acquisitions with EPI. This method has been validated in rat brain by comparison of multi-modal maps obtained by using the two-point and multi-point fitting approaches during varied levels of activity, and the basic theory and associated experimental/systematic errors for multi-slice imaging have been discussed.[36] By use of an MRI contrast agent and repeated measurements of changes in R_2 and R_2* with stimulation (in the same subject), the CBV changes can be determined with the same method. Prior to the start of data acquisition a DANTE method[26] was used to calculate $R_2^*(\Delta B_o)$[23,24] and to be used in eqn (2) to determine $\Delta R_2'(Y)$ for calculating ΔS/S [see eqn (3)]. The BOLDED AFFAIR sequence was initiated with a *TR* of 64 s (eight raw images, where each image was acquired every 8 s). The first and last five images represented the control conditions, whereas during the middle five images the rat experienced forepaw stimulation. In each rat, this protocol was repeated with and without the MRI contrast agent AMI-227. The R_1 data obtained (at rest and during activation) without the contrast agent were used to calculate CBF maps, whereas the R_2* and R_2 maps (at rest and during activation) obtained without the contrast agent were used to calculate BOLD signal-changes. The R_2* and R_2 maps (at rest and during activation) obtained with and without the contrast agent were used to calculated the CBV changes. CMR_{O2} maps were created based on eqn (8) [or eqn (10)].

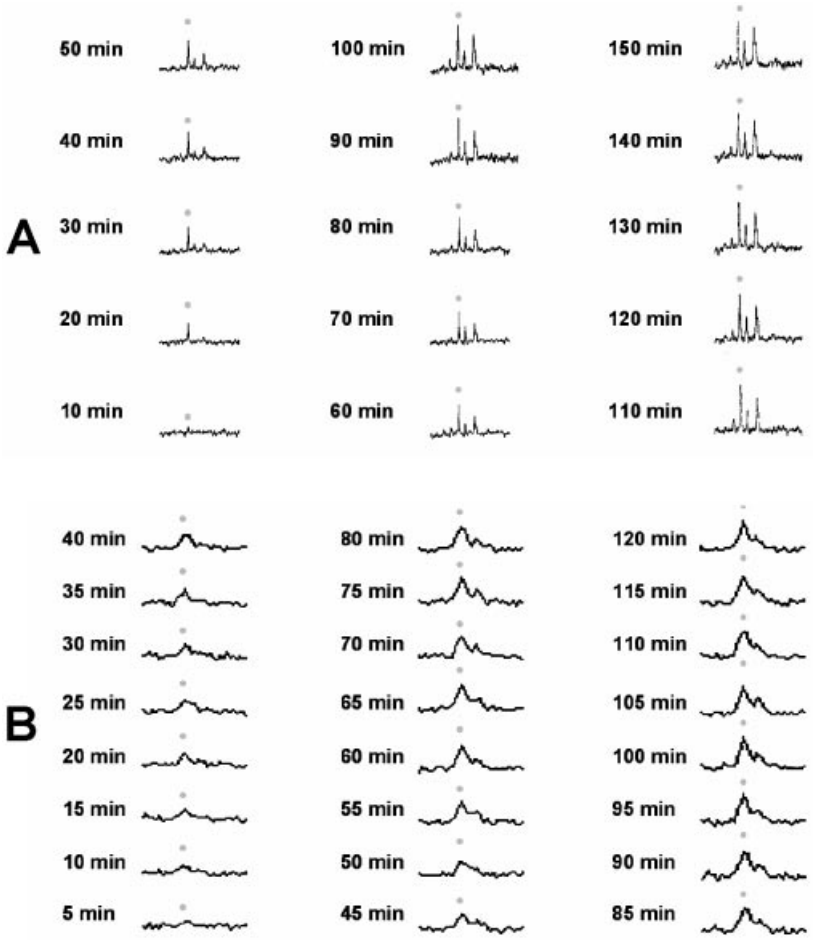

Figure 3. Typical ^{13}C turnover spectral data from (A) direct ^{13}C and (B) indirect ^{13}C (i.e. POCE) experiments localized in the somatosensory area of α-chloralose anesthetized rats (group δ), where the chemical shift position of C4-glutamate is shown with a gray dot. These spectra were exponentially line-broadened by 10–20 Hz. The V_{TCA} determined from the time-courses of C4-glutamate were similar for both rats, and are in good agreement with previous measurements.[7,13,16,17]

RESULTS

Measurements of cerebral metabolism and perfusion by MRS and MRI methods

Serial spectra obtained from the somatosensory region of rat brain by direct and indirect ^{13}C MRS methods are shown in Fig. 3 for α-chloralose anesthetized rats (group δ) during [1-^{13}C]glucose infusion. The time-courses of C4-glutamate signal increase were similar for both rats (i.e. V_{TCA} of 0.44 ± 0.05 and 0.49 ± 0.08 μmol/g/min) indicating that both methods have comparable sensitivity towards ^{13}C turnover in glutamatergic neurons of cerebral cortex. Although the spectral resolution of direct ^{13}C data is notably superior, the main advantage of the indirect method for ^{13}C turnover of C4-glutamate is the spatial resolution (i.e. ~50 μl and ~300 μl for indirect and direct ^{13}C, respectively) since the ^{13}C signal is detected at the sensitivity of ^{1}H. The sensitivity of POCE has increased several-fold in the last few years,[13,16,17,37,38] and recently indirect ^{13}C in conjunction with chemical shift imaging has been implemented using ICED PEPSI to obtain 8 μl voxels in rat cortex.[19,20] Typical ICED PEPSI data for ^{13}C detection of C4-glutamate *in vivo* in 8 μl voxels used for CMR_{O2} mapping is shown in Fig. 4 and compared with BOLD [shown in terms of an $R_2'(Y)$ map as in eqn (2)] CBF and CBV maps (from the same rat: group α). The CBV map is represented by a spin-echo MRI which reveals the distribution of the MRI contrast agent (AMI-227) at baseline. Although the spatial resolution in the CMR_{O2} map is lower than the other MRI-derived maps, the observed regional correlations of metabolism (by MRS), perfusion (by MRI), and BOLD signal support neurovascular coupling.[39,40]

Figure 5 shows typical metabolic and perfusion data obtained from rat brain in the different conditions:[13] control condition of morphine anesthesia (group α),

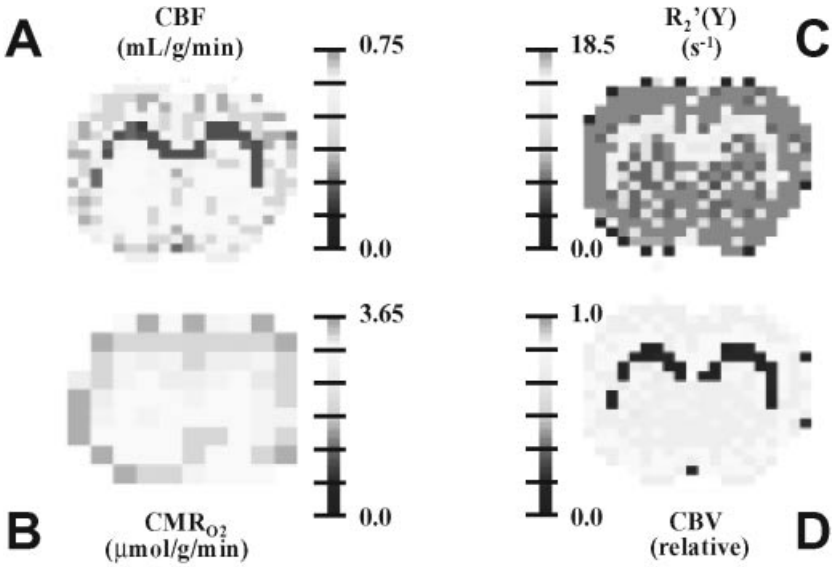

Figure 4. High-resolution multi-modal MRI and MRS data of (A) absolute CBF, (B) absolute CMR_{O2}, (C) absolute $R_2'(Y)$, and (D) relative CBV maps from rat brain. Each measurement was made under steady-state metabolism and perfusion in the *same* rat under morphine anesthesia (group α). The scale bars in (A)–(C) represent absolute units of CBF (ml/g/min), CMR_{O2} (μmol/g/min), and $R_2'(Y)$ (s^{-1}), respectively, whereas the scale bar in (D) represents a relative scale of resting CBV. The nominal spatial resolutions in (A), (C) and (D) were $320 \times 320 \times 1000\ \mu m^3$, whereas in (B) was $1250 \times 1250 \times 5000\ \mu m^3$. As shown, the data were differently interpolated

followed by either pentobarbital administration (group β), or nicotine infusion (group γ); another control condition was α-chloralose anesthesia (group δ), followed by forepaw stimulation (group ε). Figure 5(A) demonstrates that, relative to 'control I' condition (group α), V_{TCA} and CBF are lowered with pentobarbital (group β; i.e. 'deactivation') and increased with nicotine (group γ; i.e. 'activation I'). Figure 5(B) demonstrates that relative to 'control II' condition (group δ), V_{TCA} and CBF are increased with forepaw stimulation (group ε; i.e. 'activation II') with a mean value of 0.7 ± 0.2 for f (see 'Protocols and methods for BOLD calibration studies' in Materials and Methods). Since the ^{13}C fractional enrichment ratio of C4-glutamate/C1-glucose at the end of each experiment for each condition was insignificantly different from the others (0.4 ± 0.1),[13] the ^{12}C dilution of the acetyl CoA pool was constant over a wide range of cerebral metabolism.

The changes in CBV (measured by MRI) and CMR_{O2} (measured by MRS) are compared with changes in CBF (measured by MRI) in Fig. 6(A). The relative changes in CBV for the global perturbations (groups β and γ) were small, ranging from 2 to 7% with respect to the 'control I' condition (group α), whereas the localized changes in CBV measured during forepaw stimulation (group ε) were slightly larger, ranging from 7 to 21% with respect to the 'control II' condition (group δ). The relationship between CBV and CBF [eqn (9)] shows that, although the relative magnitudes in CBV changes for the two control conditions (groups α and δ) were different (i.e. 5 ± 3 vs $14 \pm 9\%$), the value of φ determined from eqn (9) was of the same magnitude (i.e. 0.10 ± 0.06) for all perturbations. Therefore, the relative changes in CBV in relation to the absolute changes in CBF could be scaled to the awake resting CBF value for the non-anesthetized resting awake condition and used in eqn (10) for the calibration. In Fig. 6(A), the changes in CBV (measured by MRI) and CMR_{O2} (measured by MRS) shows that $(\Delta CMR_{O2}/CMR_{O2}) \gg (\Delta CBV/CBV)$ over the same range of changes in CBF (measured by MRI). Because the measured $\Delta CMR_{O2}/CMR_{O2}$ values above the non-anesthetized resting awake condition [group ε; top right quadrant in Fig. 6(A)] were partial-volume corrected, a nonlinear fit over the whole dynamic range is a better representative for the relationship between CMR_{O2} and CBF [see below and Fig. 7(C)].

Probing BOLD image-contrast of glutamatergic neurons

The BOLD signal-changes [see eqn (3)] were measured for the same physiological perturbations as described in Fig. 5. Figure 6(B) shows the summary of all multi-modal MRI and MRS data which have been used to standardize the BOLD fMRI signal-changes over a wide range of

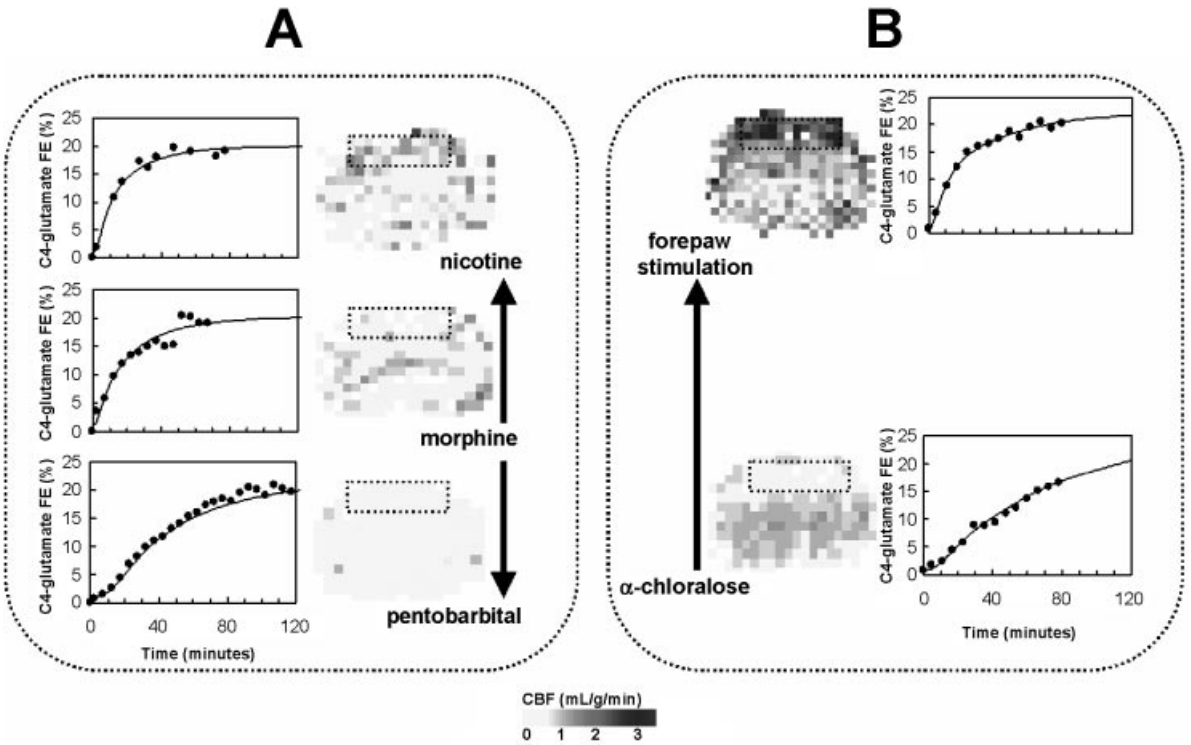

Figure 5. Measurements of CBF and V_{TCA} in the same rat, by MRI and MRS methods, for global (A) and focal (B) perturbations.[13] The color bar at the bottom shows the scaling for the CBF data, whereas V_{TCA} is depicted by the C4-glutamate time courses from the POCE data (●) and the best-fits of the metabolic model (—) to the data, where the vertical axis is the C4-glutamate ^{13}C fractional enrichment in the brain and the horizontal axis is the time after [1-^{13}C]glucose infusion began. The dotted rectangle in each CBF map represents the localized region from where the metabolic data were obtained from. (A) Group α is the 'control I' condition of morphine sulfate anesthesia ($V_{TCA} = 1.1 \pm 0.1$ μmol/g/min; CBF = 0.8 ± 0.1 ml/g/min); group β is 'deactivation' from group α with addition of sodium pentobarbital ($V_{TCA} = 0.4 \pm 0.1$ μmol/g/min; CBF = 0.3 ± 0.1 ml/g/min); and group γ is 'activation I' from Group α with infusion of nicotine hydrogen tartrate ($V_{TCA} = 1.4 \pm 0.1$ μmol/g/min; CBF = 1.1 ± 0.1 ml/g/min). (B) Group δ is 'control II' condition of α-chloralose anesthesia ($V_{TCA} = 0.5 \pm 0.1$ μmol/g/min; CBF = 0.4 ± 0.1 ml/g/min), and group ε is 'activation II' from group δ with forepaw stimulation, where $f = 0.7 \pm 0.2$ from thresholded activated CBF maps ($V_{TCA} = 1.7 \pm 0.4$ μmol/g/min; CBF = 1.6 ± 0.4 ml/g/min). The values in brackets are the mean ± standard deviation values ($n = 22$).[13] Modified from Hyder *et al.*[13,41]

neuronal activity (groups α–ε). The average contribution of ΔB_o to R_2*(obs) was $7 \pm 1\ s^{-1}$ ($n = 28$) in the region of interest.[24] The average values ($n = 28$) of Ψ, Λ and θ in eqn (7) were 0.75 ± 0.16, 0.12 ± 0.07 and 0.10 ± 0.06, respectively, to provide a standardized value of 0.36 ± 0.09 for A (TE = 26 ± 4 ms) representing the non-anesthetized resting awake condition. To gain insight into the relative importance of the oxygenation-dependent relaxation term in relation to the BOLD signal-change [eqn (1)], we defined the rate by the difference between R_2*(obs) and R_2(obs), after removal of the R_2*(ΔB_o) component,[23,24] leaving only the $R_2'(Y)$ term [see eqn (2); Appendix A]. Figure 7(A) shows that the $R_2'(Y)$ term [eqn (2)] is linearly correlated with the ratio of CMR_{O2}/CBF. This indicates a negative correlation between BOLD signal and oxygen extraction fraction (OEF), as shown in Appendix A, which has been qualitatively observed by others[42,43] and provides experimental verification for assumptions used in description of the BOLD theory.[1–5]

Figure 7(B) shows the comparison of the *predicted* $\Delta CMR_{O2}/CMR_{O2}$ [by eqn (8)] and *measured* $\Delta CMR_{O2}/CMR_{O2}$ (by POCE). Because most of the data points representing the MRI-predicted and MRS-measured values of $\Delta CMR_{O2}/CMR_{O2}$ lie close to the line of identity over a wide dynamic range of neuronal activity (groups α–ε), there is high confidence [$m = 0.9 \pm 0.1$; eqn (11)] of the BOLD fMRI signal calibration at 7 T in rat cortex ($n = 28$). Figure 7(C) indicates that CBF (measured by MRI) and CMR_{O2} (measured by MRS) change near proportionately in the rat somatosensory cortex over a wide dynamic range.[13] Because the BOLD signal calibration described above [Fig. 7(B)] is valid for the same range of activity [Fig. 7(C)], eqn (8) can be used in conjunction with multi-modal measurements of BOLD signal, CBF and CBV to calculate changes in CMR_{O2}. Figures 6 and 7 reveal that CBF and CMR_{O2} play a more dominant role in modulation of the BOLD fMRI signal at 7 T in rat cortex.

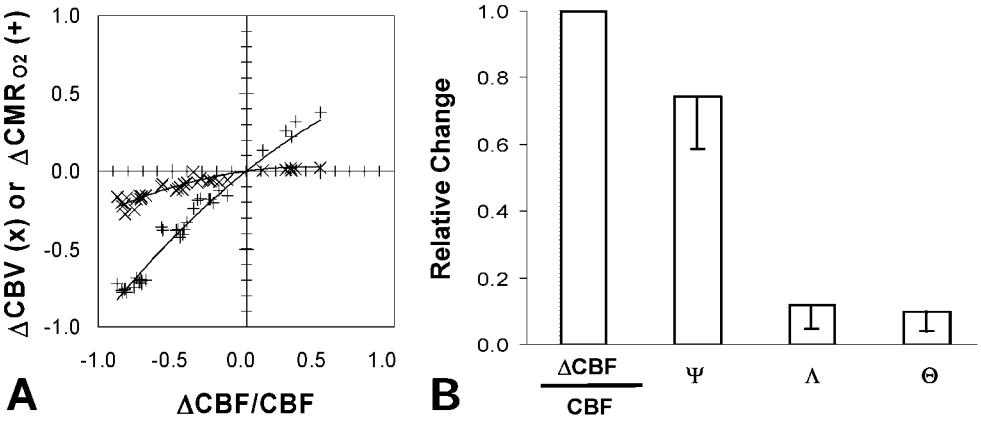

Figure 6. (A) Comparisons of $\Delta CBV/CBV$ ($\times$) and $\Delta CMR_{O2}/CMR_{O2}$ ($+$) *vs* $\Delta CBF/CBF$ for the different conditions (groups α–ε). The ratios of $(\Delta CMR_{O2}/CMR_{O2})/(\Delta CBF/CBF)$ and $(\Delta CBV/CBV)/(\Delta CBF/CBF)$, given by Ψ and Λ, respectively, in eqn (7), are significantly different (slopes through origin are $\sim$0.8 and $\sim$0.1, respectively). The origin represents the resting awake state for rat cerebral cortex.[13] Modified and updated from Hyder *et al.*[13,41] and Kida *et al.*[23,24] (B) Summary of quantitative MRI and MRS measurements of relative changes in CBF, CMR_{O2}, CBV and BOLD signal, over a wide range of neuronal activity (groups α–ε). For each condition, the changes in CBF, CMR_{O2}, CBV and BOLD signal were normalized by changes in CBF which resulted in ratios of $\Delta CBF/CBF$ (normalized to 1), Ψ, Λ and θ, respectively [eqn (7)]. This normalization procedure provides a comparison of relative changes in each parameter during changes in neuronal activity. These findings show that CBF and CMR_{O2} play a more dominant role in modulation of BOLD image-contrast at 7 T in glutamatergic neurons of rat brain. The error bars represent the standard deviation from the mean

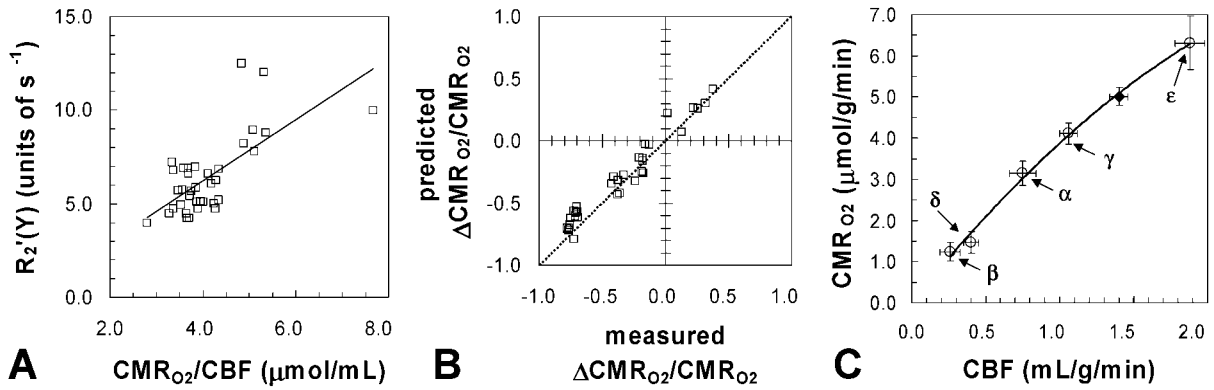

Figure 7. The neuroenergetic basis of BOLD is investigated with multi-modal MRS and MRI measurements. (A) The transverse relaxation rate term of $R_2'(Y)$, as shown in eqn (2), is positively correlated with the ratio of CMR_{O2}/CBF which is related to OEF (see Appendix A). This relationship, which has been qualitatively observed,[42,43] provides quantitative experimental verification of BOLD theory.[1–5] Modified and updated from Kida *et al.*[23,24] (B) The *predicted* $\Delta CMR_{O2}/CMR_{O2}$ [by eqn (10)] and *measured* $\Delta CMR_{O2}/CMR_{O2}$ (by POCE) values are compared to provide validation of BOLD calibration at 7 T in glutamatergic neurons of rat cerebral cortex. The dotted line represents the line of identity and a linear regression analysis of the data provides a value of $m = 0.9 \pm 0.1$ [eqn (11)] with $R^2 = 0.95$. These results indicate that at very high static magnetic fields strengths deoxygenation effects in blood dominates relaxation effects in tissue[1,2] which can be accentuated by combining the gradient-echo and spin-echo data [eqn (2)]. Since the validation of BOLD calibration relies on standard errors of independent measures for relaxation rate, blood flow, and volume, by comparing the *calculated* and *measured* $\Delta CMR_{O2}/CMR_{O2}$ it can be calculated that the validation accuracy for high-resolution CMR_{O2} mapping by multi-modal MRI at 7 T in rat cortex is at least 80%. Modified and updated from Kida *et al.*[23,24] (C) Comparison of CMR_{O2} (measured by MRS) *vs* CBF (measured by MRI) for the different conditions (groups α–ε). For the observed relationship between CBF and CMR_{O2}, the tissue pO_2 has to remain significantly lower than vessel pO_2 values,[13,44,45] which supports a situation in which the effective mass transfer coefficient for oxygen (D) must change (see Appendix C). Since the ratio of $(\Delta D/D)/(\Delta CBF/CBF)$ expressed as a constant Ω was determined to be 0.8 ± 0.2, it is suggested that the efficiency of oxygen delivery plays an important role for the regulation of oxygen delivery *in vivo*. The filled symbol represents the resting awake state for rat cerebral cortex.[13] The error bars represent the standard deviation from the mean. Modified and updated from Hyder *et al.*[13]

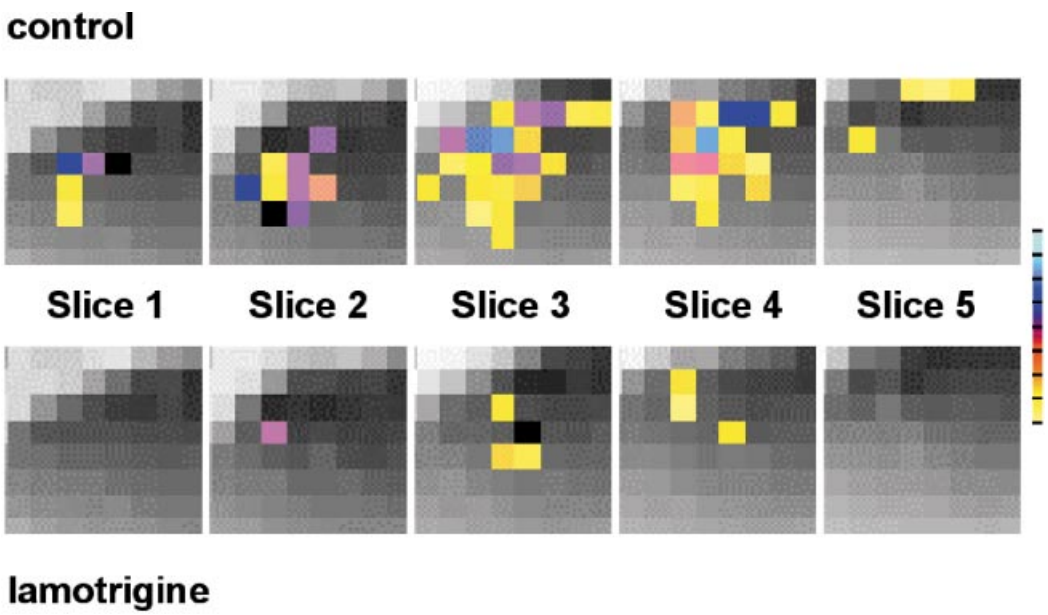

Plate 1. The neurochemical basis of BOLD is investigated with pharmacological treatment of lamotrigine, which is a neuronal voltage-dependent Na^+ channel blocker and glutamate release inhibitor.[35] Since the localized BOLD response (in the forelimb area of the somatosensory cortex in multi-slice data) during forepaw stimulation after lamotrigine treatment significantly declined (from 0.07 ± 0.01 to 0.03 ± 0.02 after lamotrigine induction; $n = 6$), the activation of voltage-dependent Na^+ channels and neuronal glutamate release are involved in the BOLD fMRI response during somatosensory activation of the rat cortex. The localized BOLD responses were obtained by averaging activated pixels across slices that remained above the same statistical threshold. The color bar represents a *t*-scale thresholded at $p < 0.01$ (yellow)

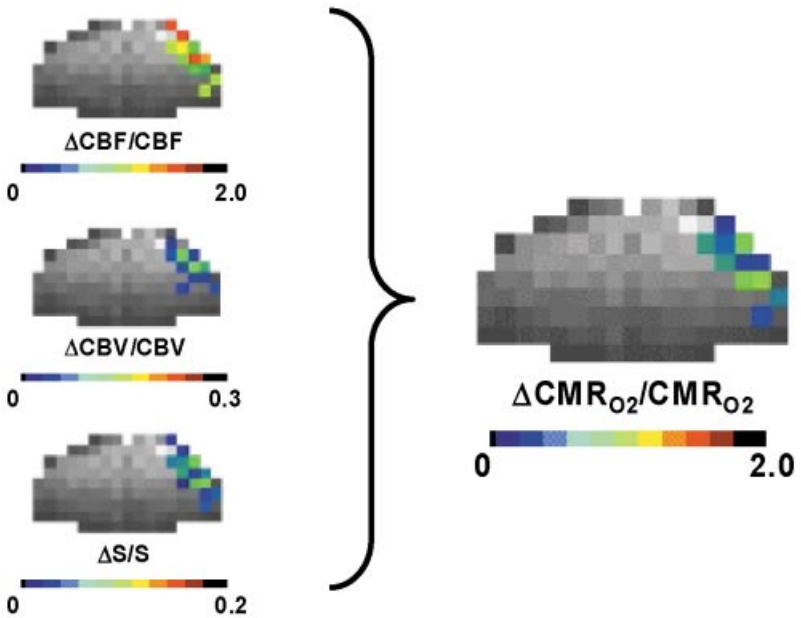

Plate 2. Multi-modal maps of localized changes in CBF, CBV, and BOLD signal (eqn 3) obtained during forepaw stimulation in an α-chloralose anesthetized rat which were used to calculate a relative CMR_{O2} map using eqn 8. The rats in this group ($n = 4$) received an initial α-chloralose dose of 40 mg/kg (i.p.). The magnitude of changes in CBF, CBV and BOLD signal were 1.17 ± 0.41, 0.07 ± 0.04 and 0.06 ± 0.02, respectively, and the localized change in CMR_{O2} was 0.93 ± 0.33 for this rat only (2×2 voxel focus). Each map is scaled differently. The regional correlation observed between changes in CMR_{O2} and CBF is very similar to regional correlation between changes in CMR_{glc} and CBF for the same rat model.[46]

To investigate the neurochemical basis of BOLD fMRI signal, pharmacological treatment with lamotrigine, which is a neuronal voltage-dependent Na^+ channel blocker and glutamate release inhibitor, was used in the rat forepaw stimulation model.[35] The magnitudes of BOLD and CBF responses to forepaw stimulation declined in a time-dependent manner within the first 2 h after lamotrigine treatment. The increases in BOLD and CBF during stimulation were reduced by ~50 and ~90%, respectively, after lamotrigine treatment. Plate 1 (Figure 8) shows the localized BOLD response during forepaw stimulation before and after lamotrigine treatment in the same rat, where the BOLD signal-change declined from 0.07 ± 0.01 before lamotrigine injection to 0.03 ± 0.02 after lamotrigine induction ($n = 6$). These results suggest that activation of voltage-dependent Na^+ channels are involved in the BOLD fMRI response.

CMR_{O2} mapping by calibrated BOLD fMRI

Plate 2 (Figure 9) shows the mapping of localized changes in CBF, CBV, and BOLD signal [using $R_2'(Y)$ as in eqn (3)] during forepaw stimulation in a lightly anesthetized rat. The magnitude of localized changes in CBF, CBV and BOLD signal were 1.22 ± 0.45, 0.08 ± 0.05 and 0.06 ± 0.02, respectively ($n = 4$). Comparison of the localized changes in CBV and CBF shows that the value of φ for the functional data (~0.1) in this lightly anesthetized condition is in agreement with the other conditions measured in Fig. 6(A) (see above). Therefore, eq. (10) could be used with the high confidence of the linear regression in Fig. 7(B) ($R^2 = 0.95$) to predict regional alterations in CMR_{O2} from the localized changes in CBF and BOLD signal and the experimentally determined values of $\acute{A}$ [eqn (7)] and φ [eqn (9)]. The regional alterations in CMR_{O2} was estimated to be 0.97 ± 0.36 using eqn (10) for the lightly anesthetized condition ($n = 4$). Alternatively, using eqn (8) with fractional changes in CBF, CBV and BOLD signal yielded insignificantly different predictions of $\Delta CMR_{O2}/CMR_{O2}$ (0.97 ± 0.36 *vs* 0.93 ± 0.40; $p > 0.3$). While magnitudes of changes in CBF and CMR_{O2} were smaller than previous values for forepaw stimulation,[13] the value of Ψ [eqn (7)], which is given by the ratio of $(\Delta CMR_{O2}/CMR_{O2})/(\Delta CBF/CBF)$ for the lightly anesthetized condition in the current study (0.7 ± 0.3), is in good agreement with previous observations[13] under deeper anesthesia (0.8 ± 0.2).

DISCUSSION

The main goal of functional imaging methods is to delineate neural processes from the neuroimaging signals. This papers deals with quantitative functional imaging studies of rat brain by MRI and MRS methods which are directed towards mapping neuronal activity by BOLD fMRI. Since ^{13}C MRS can provide measurements of brain energy metabolism, we review some methodological details of the method for neuroenergetics. Multimodal experiments which deal with the neurophysiological basis of BOLD fMRI are also discussed in detail. Methodological pitfalls of perfusion (CBF and CBV) imaging by MRI methods are discussed elsewhere.[13,24,27–30] Consequences of these results and use of these methods for high-resolution CMR_{O2} (i.e. neuronal activity) mapping by BOLD fMRI are discussed.

Measurements of neuroenergetics using ^{13}C MRS

^{13}C MRS provides a unique window on cerebral metabolism of ^{13}C labeled glucose[6,7,9,33] (Fig. 1). In contrast to ^{14}C isotopes detected in 2-deoxyglucose autoradiography,[8] ^{13}C isotopes in conjunction with ^{13}C MRS allow measurement of one or more metabolites at different carbon positions in real time. Furthermore, placement of ^{13}C label in different carbon positions of a substrate can also provide information about fluxes through different enzymes. For example, [1-^{13}C]glucose and [2-^{13}C]glucose experiments are used to measure fluxes through pyruvate dehydrogenase and pyruvate carboxylase, which are localized in the neuron and astrocyte, respectively[7] (Fig. 2). Since the enzymes for glutamate and glutamine synthesis (i.e. glutaminase[51] and glutamine synthetase,[52] respectively) are localized in the neuron and astrocyte, respectively, glutamate and glutamine are considered neuronal and astrocytic pools.[53–57]

In the studies used to calibrate the BOLD effect at 7 T for CMR_{O2} determination in rat brain (Figs 3–7), the rate of neuronal glucose oxidation was determined from ^{13}C labeling of C4-glutamate during infusion of [1-^{13}C]glucose. In this experiment the ^{13}C label flows from C1-glucose to C3-pyruvate and C3-lactate, via the tricarboxylic acid cycle intermediates, into C4-glutamate due to fast isotopic exchange between C4-glutamate and C4-α-ketoglutarate, and finally into C4-glutamine due to glutamate release by the neuron and uptake by the astrocyte[6] (i.e. neurotransmitter cycling). As long as [1-^{13}C]glucose infusion is continuous under steady-state conditions, the first turn of the tri-carboxylic acid cycle will always lead to the scenario described above. Because C4-glutamine labeling lags behind C4-glutamate under these situations, the [1-^{13}C]glucose experiment mainly reflects neuronal pyruvate dehydrogenase activity (i.e. neuronal glucose oxidation). A [1,6-^{13}C]glucose experiment is identical to a [1-^{13}C]glucose experiment except that the ^{13}C fractional enrichment of each pool is doubled since C1,6-glucose forms two identical ^{13}C labeled trioses and labels C3-pyruvate and C3-lactate twice per glucose molecule.

The metabolic model for the [1-^{13}C] or [1,6-^{13}C]glucose experiment, which yields CMR_{O2} and $CMR_{glc(ox)}$, is schematically shown in Fig. 1[13,16,17,31,32] and elaborated in Appendix B. Several modeling parameters have secondary effects upon the calculated metabolic fluxes, and the magnitude of these effects can be evaluated by sensitivity analyses,[31,32] or have been measured in separate experiments. Since these analyses[16,17,31,32] reveal that many of these parameters have relatively small effects on V_{TCA}, CMR_{O2}, and $CMR_{glc(ox)}$ ($\pm$10% to $\pm$15%) for the dynamic range covered in our anesthetized rat studies[13] (Figs 5 and 6), the derived metabolic fluxes with [1-^{13}C] or [1,6-^{13}C]glucose can provide important information on neuroenergetics.[6,7,9,33]

The observation that glutamate is packaged within vesicles in pre-synaptic terminals[58] led to the suggestion that there may be independent *transmitter* and *metabolic* pools of glutamate that are turning over at different rates,[59] where the transmitter pool is essentially metabolically inactive, being taken up by the nerve terminal after release into the synaptic cleft. An alternative model which links the transmitter pool of glutamate directly to metabolism is the idea of cycling of glutamate and glutamine between neurons and astrocytes (i.e. glutamate-glutamine neurotransmitter cycle).[60] Several independent observations support the glutamate-glutamine cycle and argue against the idea of separate *transmitter* and *metabolic* glutamate pools:[55] active astrocytic uptake of extracellular glutamate[61] which is coupled to astrocytic glucose metabolism,[62] enzymes for glutamate and glutamine synthesis are localized in neurons and astrocytes respectively,[51,52] and the precursors of glutamate and glutamine are each other.[53–57] Recent ^{13}C MRS studies *in vivo*[6,7] have demonstrated an approximately 1:1 relationship between increases in the rates of neuronal glucose oxidation (via glutamate turnover) and neurotransmitter cycling (via glutamate and glutamine turnovers) with increasing electrical activity. Therefore, the derived metabolic fluxes with [1-^{13}C]glucose provide information on functional neuroenergetics[6,7] because the metabolic and transmitting roles of glutamate are almost completely coincident with ATP production and signal propagation by the neuron.

Regulated cerebral metabolism and perfusion

At rest, approximately 20% of energy produced in the awake human body is used in the brain, which is less than 5% in total weight.[63] It is generally believed that under normal physiological conditions in the adult mammalian brain, almost all of the energy required for ATP generation is supplied via oxidation of glucose through the tri-carboxylic acid cycle leading to oxidative phosphorylation.[48] Roy and Sherrington[40] suggested that cerebral perfusion is locally adjusted to meet the regional metabolic needs. Brain cells rely on an abundant and continuous supply of oxygen for normal function and any reduction in supply of oxygen leads to permanent neuronal damage. Therefore normal brain function requires that oxygen delivery be regulated in relation to the oxidative metabolic requirements of nerve cells.[48] An important point is that, while there is no requirement for a constant stoichiometry between changes in CBF and CMR_{O2}, there is a prescribed stoichiometric ratio between changes in CMR_{O2} and CMR_{glc} if glucose oxidation is to be maintained from rest to higher and/or lower levels of activity.[9] Our investigations in rat brain over a wide range of neuronal activity (Fig. 5) have allowed relationships between $CMR_{glc(ox)}$, CMR_{O2}, and CBF to be explored (Fig. 6), which reveals that more than 95% of neuronal ATP production is accounted for via glucose oxidation over a wide range of activity.[13] These results indicate that ATP homeostasis is maintained over a wide range of conditions by altered metabolic rates.[64]

The relationship between CMR_{O2} and CBF [Fig. 7(C)] reveals that substrate delivery is tightly associated with brain energy metabolism.[48] These results have important implications for theories on cerebral oxygen delivery.[13,44,45] Based on the assumption that the flow of oxygen across the blood-brain barrier is proportional to the partial pressure of oxygen (pO_2) in the capillary, a model was presented[44] which links CMR_{O2} to CBF (and CBV) through an effective mass transfer coefficient for oxygen (D) of the capillary bed (see Appendix C). Based upon *in vivo* evidence that the effective mass transfer coefficient for oxygen may be altered by changes in capillary pO_2, hematocrit and/or blood volume,[65–68] the model allows changes in D with changes in CBF. Choice in the model of the appropriate ratio of Ω, which is given by $(\Delta D/D)/(\Delta CBF/CBF)$, determines the dependence of tissue oxygen delivery upon perfusion. While the model does not predict any particular observed proportionality between CBF and CMR_{O2}, the model's capacity to fit the wide range of data indicates that the oxygen diffusion properties of the capillary bed, which can be modified in relation to perfusion (i.e. $1 > \Omega > 0$; see Appendix C), plays an important role in regulating cerebral oxygen delivery. The effective mass transfer coefficient for oxygen, D, is derived under the assumption that oxygen delivery is proportional to local vessel pO_2 (Appendix C). The evidence that oxygen delivery is proportional to local vessel pO_2 is based on studies[69] which have shown that tissue pO_2 is lower than vascular pO_2, and very little tissue oxygen diffuses back out into the microvasculature.[70] Measurements of tissue pO_2 suggest that under the conditions studied here it remains significantly lower than vessel pO_2 values,[69] which supports a situation in which D must change to explain the observed relationship between CBF and CMR_{O2} in Fig. 7(C).[13] The relationship between CBF and D, expressed as Ω, was determined *in vivo*[13] to be 0.8 ± 0.2 over the dynamic range. These results support an important role for the

capillary bed to modulate the efficiency of oxygen delivery *in vivo*.[44,45]

Neurophysiology of BOLD fMRI in rat brain at 7 T

The approach we employed to calibrate the BOLD image-contrast differs from previous animal studies which used non-physiological challenges (e.g. hypoxia or hypercapnia) to perturb CBF.[42,43] In previous studies the changes in CBV were assumed to follow the dependence proposed by eqn (9) for hypercapnic challenges in primates[34] and changes in CMR_{O2} and CBV were not measured. The value of φ from eqn (9) was determined to be $\sim$0.4 by Grubb *et al.*[34] in a PET study, whereas the value of φ determined in the current MRI study was $\sim$0.1 for a wide range of activity in rat brain [Fig. 6(A)]. This discrepancy could be partially attributed to different tracers used in the MRI and PET methods for CBV measurements. Because the distribution spaces and half-lives of PET and MRI tracers are different, the changes in tracer kinetics of each label reflect changes in different compartments of blood (e.g. plasma *vs* hemoglobin). Alternatively, hypoxia and hypercapnia induce some level of uncoupling between oxygen delivery and consumption, and alterations in blood pH and/or hematocrit,[48] which may lead to a different coupling between CBF and CBV than with physiological stimulation.

The BOLD calibration was tested by comparison of $\Delta CMR_{O2}/CMR_{O2}$ predicted [by eqn (8)] and measured (by POCE). The accuracy of the BOLD calibration in Fig. 7(B) [$m = 0.9 \pm 0.1$; eqn (11)] is consistent over a wide range of neural activity, from the deeply anesthetized condition (bottom left quadrant) to highly activated condition (top right quadrant). The highest levels of activity are above the non-anesthetized resting awake condition (origin). Although the confidence limit of calibration of the BOLD signal is quite high [Fig. 7(B)] there are limitations to the calibration. One potential source of uncertainty in comparing the MRI-predicted CMR_{O2} data [by eqn (10)] with the MRS-measured CMR_{O2} data (by POCE) is the heterogeneity in metabolism within larger MRS voxels in comparison to ΔCBF/CBF, ΔCBV/CBV, and $\Delta S/S$ measurements which all have substantially superior spatial resolution. This heterogeneity is greater under conditions of sensory stimulation than non-stimulated conditions. The CMR_{O2} measured (by POCE) in the region of interest is equivalent to the average of CMR_{O2} predicted [by eqns (8) or (10)] from all MRI sub-voxels. If theory is correct, by calculating $\Delta CMR_{O2}/CMR_{O2}$ in each voxel from the MRI data and then summing, the average value determined from the BOLD calibration should agree with the MRS measurement. The finding of good experimental agreement between these independent measures [Fig. 7(B)] strongly supports the combined use of BOLD signal, CBF and CBV measurements to map CMR_{O2} at 7 T (see below; Plate 2 (Figure 9)). However, a limitation in this approach is that voxels at the MRI spatial resolution with very high or low values of CMR_{O2}, which may not be reliably characterized by the BOLD calibration, could be averaged out. Since calibrating the BOLD effect [eqn (11)] is limited by standard errors in independent measures of relaxation rate, blood flow and volume (maximally expected to be $\pm$5, $\pm$10 and $\pm$5%, respectively[24]), by comparing the *calculated* $\Delta CMR_{O2}/CMR_{O2}$ with the *measured* $\Delta CMR_{O2}/CMR_{O2}$ (where the associated errors are within $\pm$15% at maximum[13]) we conclude that the validation accuracy for neuroenergetics of BOLD image-contrast at 7 T is at least 80%.

We expect the accuracy of the BOLD calibration at 7 T in the rat cortex to be high over a wide range of neuronal activity [Fig. 7(B)] because of the linear relationship observed between CBF and CMR_{O2} over the same range. Figure 7(C) indicates that CBF (measured by MRI) and CMR_{O2} (measured by MRS) change nearly proportionately in the rat somatosensory cortex over a wide dynamic range.[13] Since the normalization of the BOLD signal described above is valid for the same range of activity [Fig. 7(B)], eqn (8) can be used in conjunction with multi-modal measurements of BOLD signal, CBF and CBV to calculate changes in CMR_{O2}. While use of the long half-life superparamagnetic MRI contrast agent for the CBV measurements[27,28] provides valuable data in these experiments, the use of these agents for human experiments is not yet approved. Alternatively, BOLD and CBF data can be used in conjunction with experimentally derived values of $\mathring{A}$ and φ to calculate changes in CMR_{O2} [eqn (10); see Plate 2 (Figure 9)]. Recent BOLD fMRI experiments in the awake human visual cortex[71,72] and in the anesthetized rat sensorimotor cortex[36,73] have shown that $\Delta S/S$ and ΔCBF/CBF are linearly correlated. These observations, in conjunction with eqn (8), indicate that the relationship between ΔCBF/CBF and $\Delta CMR_{O2}/CMR_{O2}$ would also be linear with functional activation as we have observed experimentally in the rat cortex [Fig. 7(C)].

Since the linear relationship between CBF and CMR_{O2} has been observed in rat and human cortex under a variety of conditions,[44,45] this BOLD calibration approach may be applied to human studies. Recent fMRI studies by Hoge *et al.*[11] and Kim *et al.*[12] in the human visual cortex also suggest a linear relationship between CBF (measured by MRI) and CMR_{O2} (predicted by MRI), where the predicted value of Ψ [eqn (7)] given by the ratio of $(\Delta CMR_{O2}/CMR_{O2})/(\Delta CBF/CBF)$ ranged from 0.5 to 0.7, which is in good agreement with the value of Ψ in the current rat studies (0.7 ± 0.3). The slight difference in the relationship between CBF *vs* CMR_{O2} for rats and humans may be due to an actual species difference in the mechanisms of cerebral oxygen delivery. However, experimentally measured values of $\mathring{A}$

and φ along with some validation experiments in human brain studies may improve the agreement between the rat and human data.

Much of BOLD fMRI research interest pertains to measurements of activation-dependent changes in the physiological parameters mentioned above (e.g. see other papers in this issue). Thus it is important to characterize the molecular mechanisms linking the observed BOLD signal-change to neurophysiology at the cellular level. Under physiological conditions Ca^{2+} dependent vesicular release of neurotransmitters (e.g. an excitatory amino acid like glutamate) occurs in response to depolarization which results from influx of Na^+ ions through presynaptic voltage-dependent Na^+ channels.[74] Neuronal excitability and neurotransmitter release can both be suppressed by inhibitors of these channels and the Na^+ current that these channels mediate. Thus Na^+ channel blockers can be applied in treatment of epilepsy and other neurodegenerative disease where excessive release of neurotransmitters is believed to contribute to neuronal injury.[75,76] The hypothesis that activation of voltage-dependent Na^+ channels is a necessary step in the neurochemical pathway leading to the BOLD and CBF responses during somatosensory activation in rat was tested.[35] After lamotrigine treatment, significant depression of localized hemodynamic and neuroenergetic responses (see Fig. 8) imply that voltage-dependent Na^+ channels is involved in the BOLD fMRI response, although more studies are required to determine the extent to which glutamate release or other neurotransmitters and modulators are involved in the generation of the BOLD neuroimaging signal.[35]

High-resolution CMR_{O2} mapping by calibrated and validated BOLD fMRI

Using the description of BOLD theory shown in Appendix A, the fractional changes in CMR_{O2} were calculated by eqn (8) where we defined the transverse relaxation rate by eqn (2). There was good agreement between *measured* and *predicted* values of $\Delta CMR_{O2}/CMR_{O2}$ [Fig. 7(B)], which strongly supports theoretical description of BOLD theory.[1–5] A detailed discussion of the biophysical consequences of these results has been described earlier.[24] In summary, the results indicate that the strongest modulator of the BOLD fMRI signal is the $R_2'(Y)$ component [eqn (2)], utilized here by differencing of R_2*(obs) and R_2(obs) after removal of the R_2*(ΔB_o) term, which is associated with the extravascular compartment at high static magnetic field strength.[1–5] At the optimal *TE* and within the physiologic range of water diffusion coefficients, gradient-echo contrast is sensitive to both small and large vessels, whereas spin-echo contrast is more sensitive to small vessels because the motional narrowing effects in large vessels are refocused [see eqns (A11) and (A12) in Appendix A[4,24]]. At a static magnetic field strength of 4 T and higher, the effects of BOLD on gradient-echo and spin-echo MRI signals are predominantly associated with the extravascular compartment,[1–5] which may provide localization of neural activation.[77]

Plate 2 (Figure 9) shows an example of quantitative high-resolution CMR_{O2} mapping in rat brain at 7 T during functional activation of the forepaw. The regional correlation between changes in CMR_{O2} and CBF observed here supports the concept of neurovascular coupling.[39,40] The correlation of region specific perfusion and metabolism has been observed during functional activation elicited by forepaw[46] and whisker[78] stimulations in anesthetized rats using [^{14}C]-2-deoxyglucose autoradiography. Furthermore, ultra-high resolution [^{14}C]-2-deoxyglucose autoradiography studies[79] have revealed that the neuropil is the site of the highest metabolic activity. These autoradiography and MRI/MRS studies suggest that functional neuroenergetic response of glutamatergic neurons can be represented to a great extent by changes in neuronal glucose oxidation. Since the BOLD effect at 7 T has been validated within 80% accuracy [see Fig. 7(B) and above]. BOLD maps can represent neuronal glucose oxidation as suggested by regional correlation between changes in CMR_{O2} and CBF during functional activation (Plate 2 (Figure 9)).

CONCLUSIONS

The BOLD image-contrast in rat cortex at 7 T has been calibrated by multi-modal MRI measurements, and the neuroenergetic weighting of the BOLD effect has been validated with the ^{13}C MRS measurements of CMR_{O2} (i.e. neuronal activity) over a wide range of activity. In support of the neurovascular coupling concept, regional correlation was observed for changes in CMR_{O2} and CBF with functional activation. Physiological and pharmacological studies reveal that BOLD signal-changes are closely linked with alterations in neuronal glucose oxidation and neuronal glutamate release. Although the exact cellular processes that underlie the BOLD phenomenon are yet to be revealed, the current findings strongly confirm the neuroenergetic and neurochemical makeup of BOLD and indicate the necessary steps towards mapping neuronal activity by fMRI.

Acknowledgements

The authors would like to thank Professor Robert G. Shulman for helpful discussions. The authors also thank engineers T. Nixon, P. Brown and S. McIntyre for maintenance of the spectrometer and the radio-frequency probe designs, and B. Wang and J. Wall for technical

support. Supported by National Institutes of Health grants NS-32126 (DLR), HD-32573 (KLB), NS-34813 (KLB), and NS-37203 (FH); and a National Science Foundation grants DBI-9730892 (FH) and DBI-0095173 (FH).

APPENDIX A. PHYSIOLOGICAL BASIS OF BOLD fMRI SIGNAL USING FICK'S RELATIONSHIP

The equilibrium between deoxyhemoglobin and oxyhemoglobin (Hb and HbO_2) can be shifted[47] by altering the blood oxygenation,

$$\mathrm{Hb(O_2)}_n \rightleftharpoons \mathrm{Hb} + n\mathrm{O_2} \tag{A1}$$

where $4 \geq n > 1$. Since Hb and HbO_2 are paramagnetic and diamagnetic respectively, BOLD image-contrast is materialized because hemoglobin acts as an endogenous MRI contrast agent. The blood oxygenation, Y, is based on the oxygen dissociation curve for hemoglobin which describes the chemical reaction of eqn (A1) at equilibrium

$$Y = \frac{C_{\mathrm{Hb(O2)n}}}{C_{\mathrm{Hb(O2)}n} + C_{\mathrm{Hb}}} \tag{A2}$$

where $C_{\mathrm{Hb(O2)}n}$ and C_{Hb} are $[\mathrm{Hb(O_2)}_n]$ and [Hb], respectively. If the sum of $(C_{\mathrm{Hb(O2)}n} + C_{\mathrm{Hb}})$ is equal to the total hemoglobin (i.e. $C_{\mathrm{Hb(total)}}$) then

$$1 - Y = \frac{C_{\mathrm{Hb}}}{C_{\mathrm{Hb(total)}}} \tag{A3}$$

Since the capillary arteriovenous oxygen difference is given by $(C_a - C_v)$ and the arterial oxygenation is assumed to be very close to 1, then it can be shown that

$$C_a - C_v = C_{\mathrm{Hb}} \tag{A4}$$

and

$$C_a \equiv C_{\mathrm{Hb(total)}} \tag{A5}$$

Then eqn (A3) rearranges to

$$1 - C_v/C_a = 1 - Y \tag{A6}$$

Since Crone[47] has shown that the oxygen extraction fraction [$\mathrm{OEF} \equiv \mathrm{CMR_{O2}}/(\mathrm{CBF} \times C_a)$] is given by

$$\mathrm{OEF} = 1 - C_v/C_a \tag{A7}$$

then eqn (A6) rearranges to

$$\mathrm{OEF} = 1 - Y \tag{A8}$$

When fractional changes in OEF are considered due to a physiologic perturbation,

$$\frac{\Delta \mathrm{OEF}}{\mathrm{OEF}} = -\frac{\Delta Y}{1 - Y} \tag{A9}$$

The BOLD fMRI signal[3–5] is defined as

$$S = S_o \exp[-TE \times R_2'(Y)] \tag{A10}$$

where TE is the echo time, $R_2'(Y)$ is the transverse relaxation rate of tissue water to be described below, and S_o is the signal at TE of zero. The relaxation rates observed with gradient-echo and spin-echo MRI are

$$R_2^*(\mathrm{obs}) = R_2'(Y) + R_2(Y) + R_2(\mathrm{other}) + R_2^*(\Delta B_o) \tag{A11}$$

$$R_2(\mathrm{obs}) = R_2(Y) + R_2(\mathrm{other}) \tag{A12}$$

where $R_2'(Y)$ and $R_2(Y)$ are the reversible and non-reversible relaxation components due to blood oxygenation effects on tissue water relaxation rate, $R_2^*(\Delta B_o)$ is the relaxation component attributed to static magnetic field distortions (ΔB_o), and R_2(other) is the relaxation component assigned to non-susceptibility-based effects. The difference between R_2^*(obs) and R_2(obs), after removal of the $R_2^*(\Delta B_o)$ component[23,24] as shown by eqn (2) in the main text, leaves only the $R_2'(Y)$ term which is devoid of the common and unknown terms between R_2^*(obs) and R_2(obs) with only the pure oxygenation term which can be described by eqn (4)[1–5] in the main text. Since $R_2'(Y)$ in eqn (A10) varies as a function of blood oxygenation level, hemoglobin acts as an endogenous MRI contrast agent. The relationship between Y, CBF and $\mathrm{CMR_{O2}}$ may be derived from Fick's principle[48]

$$\mathrm{CMR_{O2}} = \mathrm{CBF} C_{\mathrm{Hb(total)}} (1 - Y) \tag{A13}$$

and the fractional changes in CBF and $\mathrm{CMR_{O2}}$ are related to the oxygenation changes

$$\left(\frac{\Delta Y}{1 - Y}\right) = \left(\frac{\Delta \mathrm{CBF}}{\mathrm{CBF}} - \frac{\Delta \mathrm{CMR_{O2}}}{\mathrm{CMR_{O2}}}\right)\left(1 + \frac{\Delta \mathrm{CBF}}{\mathrm{CBF}}\right)^{-1} \tag{A14}$$

Given the baseline BOLD signal by eqn (A10), it can be shown that a perturbation leads to an expression for $\Delta S/S$ as shown by eqn (3) in the main text. The $\Delta R_2'(Y)$ term in eqn (3) in the main text can be expanded from the relationship of eqn (4) in the main text

$$\left(1 + \frac{\Delta R_2'(Y)}{R_2'(Y)}\right) = \left(1 - \frac{\Delta Y}{1 - Y}\right)\left(1 + \frac{\Delta b}{b}\right) \tag{A15}$$

which can be expanded further based on eq. [A.14] to

show the physiological basis of $\Delta R_2'(Y)$

$$\Delta R_2'(Y) = \left[\left(1+\frac{\Delta \mathrm{CMR_{O2}}}{\mathrm{CMR_{O2}}}\right)\left(1+\frac{\Delta \mathrm{CBV}}{\mathrm{CBV}}\right)\left(1+\frac{\Delta \mathrm{CBF}}{\mathrm{CBF}}\right)^{-1}-1\right]R_2'(Y)$$

where $\acute{A}$ in eqn (1) is given by the product of $R_2'(Y)$ and TE.

APPENDIX B. DETERMINATION OF CMR_{O2} AND $CMR_{glc(ox)}$ BY ^{13}C MRS

If glucose is the only source of carbon for the tricarboxylic acid cycle and all the [1-^{13}C]glucose enters the acetyl CoA pool, then the stoichiometry of fluxes for the breakdown of glucose is given by

$$\mathrm{CMR_{glc}} = 1/2 V_{\mathrm{TCA}} \quad \text{(B1)}$$

$$\mathrm{CMR_{O2}} = 3V_{\mathrm{TCA}} \quad \text{(B2)}$$

and the ^{13}C fractional enrichment of C4-glutamate should be exactly half that of C1-glucose. However, experimentally we find that ^{13}C fractional enrichment of C4-glutamate is less than half that of C1-glucose.[7,13,16,17,31,32] Two metabolic pathways that may contribute to the dilution of C4-glutamate are ^{12}C influxes from ketone bodies, V_{ket}, and pyruvate (and lactate) blood-brain exchange, V_{ex}, both of which contribute unlabeled carbons to the acetyl CoA pool. V_{out} represents a net efflux of pyruvate (and lactate) into the blood from the brain.[9] Under these conditions, the mass balance between V_{TCA} and $\mathrm{CMR_{glc}}$, based on the fact that a hexose forms two trioses, is given by

$$\mathrm{CMR_{glc}} = 1/2[V_{\mathrm{TCA}} - V_{\mathrm{ket}} + V_{\mathrm{out}}] \quad \text{(B3)}$$

where the *oxidative* portion is

$$\mathrm{CMR_{glc(ox)}} = 1/2[V_{\mathrm{TCA}} - V_{\mathrm{ket}}] \quad \text{(B4)}$$

and the *non-oxidative* portion is

$$\mathrm{CMR_{glc(non-ox)}} = 1/2 V_{\mathrm{out}} \quad \text{(B5)}$$

Although V_{out} cannot be measured by this approach, by comparison of $\mathrm{CMR_{glc(ox)}}$ from ^{13}C MRS and $\mathrm{CMR_{glc}}$ from autoradiography under a variety of conditions[13,16,17] can allow the determination of $\mathrm{V_{out}}$ [i.e. $\mathrm{CMR_{glc(ox)}}$ as in eqn (B5)]. Likewise, the stoichiometry between V_{TCA} and $\mathrm{CMR_{O2}}$ is given by

$$\mathrm{CMR_{O2}} = 3[2\mathrm{CMR_{glc}} - V_{\mathrm{out}}] + 2\,1/4 V_{\mathrm{ket}} \quad \text{(B6)}$$

where the different factors for [2 $\mathrm{CMR_{glc}} - V_{\mathrm{out}}$] and V_{ket} in eqn (B6) signify that different precursors for acetyl CoA (i.e. glucose and ketone bodies) are coupled differently to oxidative metabolism.[31,32] Substituting eqn (B3) into (B6) results in

$$\mathrm{CMR_{O2}} = 3V_{\mathrm{TCA}} - 3/4 V_{\mathrm{ket}} \quad \text{(B7)}$$

which calculates the oxygen consumption from the tricarboxylic acid cycle. Therefore, for each value of V_{TCA} the values of $\mathrm{CMR_{glc(ox)}}$ and $\mathrm{CMR_{O2}}$ can be calculated from eqns (B4) and (B7), respectively. The value of total dilution of the acetyl CoA pool, $\mathrm{V_{dil}}$, is given by

$$V_{\mathrm{dil}} = V_{\mathrm{TCA}} \frac{1 - [\text{C4-glutamate } ^{13}\text{C fractional enrichment}]}{\mu[\text{glucose } ^{13}\text{C fractional enrichment}]} \quad \text{(B8)}$$

provided that the enrichment of the glutamate pool has reached steady-state (where $\mu = 1/2$ and 1 for [1-^{13}C]glucose and [1,6-^{13}C]glucose experiments, respectively).

APPENDIX C. MODEL OF CEREBRAL OXYGEN DELIVERY AND ITS RELATION WITH BOLD fMRI

The oxyhemoglobin dissociation curve [eqn (A2)] describes the oxygen carrying propensity of blood. The amount of oxyhemoglobin, $C_{\mathrm{Hb(O2)}n}$, is in equilibrium with deoxyhemoglobin, C_{Hb}, and oxygen, C_{O2} [eqn (A1)]. The model[44,45] proposes that for a given microscopic capillary segment the rate of oxygen delivery is proportional to the vessel-to-tissue pO_2 gradient. Most of the dissolved oxygen molecules that cross the blood- brain barrier radially diffuse into the tissue and are consumed. The maximum vessel pO_2 is equal to the pO_2 of arteriolar blood and oxygen diffusion constant is hypothesized to be constant. Extraction of oxygen into the tissue from an infinitesimally thin blood bolus occurs all through transit, where the temporal profile of the total oxygen content of blood (C_{B}) can be described in relation to the oxygen content in the plasma (C_{P}) by

$$\mathrm{d}C_{\mathrm{B}}/\mathrm{d}\tau = -k' C_{\mathrm{P}}(1-q) \quad \text{(C1)}$$

where the C_{B} is equivalent to $C_{\mathrm{Hb(O2)n}}$, C_{P} is equivalent to C_{O2}, q is related to the dissolved oxygen in the extravascular space (C_{T}) in relation to C_{P}, and the constant k' is determined by the spatial gradients of oxygen tension radially around the bolus, and is the first-order rate constant of oxygen loss from the capillary. The main assumptions in eqn (C1) have been described.[44,45] If it is assumed that through an elapsed time of $\Delta\tau$ the ratio of transient oxygen contents in plasma and blood is constant, i.e. $r = C_{\mathrm{P}}/C_{\mathrm{B}}$, then

$$C_{\mathrm{B}}(\tau + \Delta\tau) = C_{\mathrm{P}}(\tau)\exp(-kr\Delta\tau) \quad \text{(C2)}$$

where k is given by the product of k' and $(1-q)$ and $\Delta\tau$ is the mth equivalent fraction of the circulation time (T_{c}).

Equation (C2) leads to

$$C_B(T_c) = C_P(0)\exp(-[kr]_{net}T_c) \quad \text{(C3)}$$

where $[kr]_{net}$ is the net-averaged kr product. The hypothetical resistance of oxygen transport is distributed over a range of physiological episodes which occur in various locations and/or phases of oxygen transport, which together are termed as the effective mass transfer coefficient for oxygen [see eqn (C7)], rather than one particular site and/or period. Oxygen extraction around the capillary may be calculated from

$$OEF_c = [C_T(0) - C_B(T_c)]/C_B(0) \quad \text{(C4)}$$

where $C_B(0) > C_B(T_c)$ and given eqn (C3), OEF_c is also equivalent to

$$OEF_c = 1 - \exp(-[kr]_{net}T_c) \quad \text{(C5)}$$

The total oxygen extraction per capillary can be depicted by the summation of the effect of an infinitesimally thin blood bolus flowing down a capillary during transit as it deposits oxygen, and as a consequence of which the flowing blood goes through changing spatial gradients of oxygen tension between the traversing volume element and the abluminal side of the blood-brain barrier. The changing values of C_T and C_P in the traversing bolus reflects the cooperative binding of oxygen by hemoglobin in whole blood within the capillary. Since perfusion is assumed to be constant all through transit, T_c is related to flowing bulk (CBV_c) and rate (CBF_c) in the circulating blood by stationarity and linearity principles,[49,50] then eqn (C5) leads to

$$OEF_c = 1 - \exp(-D_c/CBF_c) \quad \text{(C6)}$$

where D_c is theoretically defined as the effective mass transfer coefficient for oxygen from the capillary to the mitochondria which is the point of efficient consumption,

$$D_c = [kr]_{net}CBV_c \quad \text{(C7)}$$

The macroscopic picture is derived through averaging across an ensemble of capillaries. A useful parameter which pertains to the efficiency of oxygen transport across the blood–brain barrier is given by

$$\Omega = (\Delta D/D)/(\Delta CBF/CBF) \quad \text{(C8)}$$

which can be theoretically viewed as a parameter that reflects the efficiency of oxygen delivery and is hypothesized to be altered by changes in vessel pO_2 (in relation to the tissue pO_2) and the value of D. If D is constant (i.e. $\Omega = 0$), then oxygen delivery may increase only through an increase in the vessel-to-tissue pO_2 gradient. Because the maximum vessel-to-tissue pO_2 gradient is limited to the pO_2 of arterial blood, the ability to increase CMR_{O2} by increasing CBF is reduced at high perfusion rates where the average vessel pO_2 approaches the arterial value. Highly non-linear relationship between CMR_{O2} and CBF is predicted by the model with $\Omega = 0$ and these predictions are heavily dependent on basal OEF values. For the case where $\Delta D/D$ and $\Delta CBF/CBF$ are equal (i.e. $\Omega = 1$), oxygen delivery increases linearly with perfusion with no change in average vessel pO_2. However, in this case a highly linear relationship between CMR_{O2} and CBF is predicted where the changes in metabolism and perfusion are exactly proportional, with no dependence on basal OEF values. In contrast when $1 > \Omega > 0$, oxygen delivery may be increased both through an increase in vessel pO_2 and D. The prediction of this model is a linear relationship between CMR_{O2} and CBF with minimal dependence on basal OEF values. A qualitative but substantial validation of these different situations is the ability to predict the BOLD fMRI image-contrast. The changes in CMR_{O2} and CBF observed during activation reflect a decrease in OEF from its basal value (i.e. $\Delta OEF/OEF < 0$) which is equal to an increased venous blood oxygenation. An increase in BOLD fMRI signal-change ($\Delta S/S$) is consistent with a decrease in venous deoxyhemoglobin concentration and $\Delta S/S > 0$ can only be predicted with $1 > \Omega \geq 0$.

REFERENCES

1. Ogawa S, Menon RS, Kim SG, Ugurbil K. On the characteristics of functional magnetic resonance imaging of the brain. *A. Rev. Biophys. Biomol. Struct.* 1998; **27**: 447–474.
2. Ugurbil K, Adriany G, Andersen P, Wei C, Gruetter R, Hu X, Merkle H, Kim DS, Kim SG, Strupp J, Hong X, Ogawa S. Magnetic resonance studies of brain function and neurochemistry. *A. Rev. Biomed. Engng* 2000; **2**: 633–660.
3. Ogawa S, Lee TM, Barrere B. The sensitive of magnetic resonance image signals of rat brain to changes in the cerebral venous blood oxygenation. *Magn. Reson. Med.* 1993; **29**: 205–210.
4. Kennan RP, Zhong J, Gore JC. Intravascular susceptibility contrast mechanisms in tissue. *Magn. Reson. Med.* 1994; **31**: 9–21.
5. Weisskoff RM, Zuo CS, Boxerman JL, Rosen BR. Microscopic susceptibility variation and transverse relaxation: theory and experiment. *Magn. Reson. Med.* 1994; **31**: 601–610.
6. Shulman RG, Rothman DL. Interpreting functional imaging studies in terms of neurotransmitter cycling. *Proc. Natl Acad. Sci. USA* 1998; **95**: 11993–11998.
7. Rothman DL, Sibson NR, Hyder F, Shen J, Behar KL, Shulman RG. In vivo nuclear magnetic resonance spectroscopy studies of the relationship between the glutamate–glutamine neurotransmitter cycle and functional neuroenergetics. *Phil. Trans. R. Soc. Lond. B* 1999; **354**: 1165–1177.
8. Sokoloff L, Reivich M, Kennedy C, des Rosiers MH, Patlak CS, Pettigrew KD, Sakurada O, Shinohara M. The [^{14}C]deoxyglucose method for the measurement of local cerebral glucose utilization: theory, procedure, and normal values in the conscious and anesthetized albino rat. *J. Neurochem.* 1977; **28**: 897–916.
9. Shulman RG, Hyder F, Rothman DL. Cerebral energetics and the glycogen shunt: Neurochemical basis of functional imaging. *Proc. Natl Acad. Sci. USA* 2001; **98**: 6417–6422.
10. van Zijl PCM, Efefe SM, Ulatowski JA, Oja JME, Ulug AM, Traystman RJ, Kauppinen RA. Quantitative assessment of blood flow, blood volume and blood oxygenation effects in functional magnetic resonance imaging. *Nat. Med.* 1998; **4**: 159–167.
11. Hoge RD, Atkinson J, Gill B, Crelier GR, Marrett S, Pike GB. Linear coupling between cerebral blood flow and oxygen consumption in activated human cortex. *Proc. Natl Acad. Sci. USA* 1999; **96**: 9403–9408.

12. Kim SG, Rostrup E, Larsson HB, Ogawa S, Paulson OB. Determination of relative CMR_{O2} from CBF and BOLD changes: significant increase of oxygen consumption rate during visual stimulation. *Magn. Reson. Med.* 1999; **41**: 1152–1161.
13. Hyder F, Kennan RP, Kida I, Mason GF, Behar KL, Rothman DL. Dependence of oxygen delivery on blood flow in rat brain: a 7 Tesla nuclear magnetic resonance study. *J. Cereb. Blood Flow Metab.* 2000; **20**: 485–498.
14. Shaka AJ, Keeler J, Freeman R. Evaluation of new broadband decoupling sequence Waltz-16. *J. Magn. Reson.* 1983; **53**: 313–340.
15. Gruetter R, Novotny EJ, Boulware SD, Mason GF, Rothman DL, Shulman GI, Prichard JW, Shulman RG. Localized ^{13}C NMR spectroscopy in the human brain amino acid labeling from D-[1-^{13}C]glucose. *J. Neurochem.* 1994; **63**: 1377–1385.
16. Hyder F, Chase JR, Behar KL, Mason GF, Siddeek M, Rothman DL, Shulman RG. Increased tri-carboxylic acid cycle flux in rat brain during forepaw stimulation detected with ^{1}H-[^{13}C] NMR. *Proc. Natl Acad. Sci. USA* 1996; **93**: 7612–7617.
17. Hyder F, Rothman DL, Mason GF, Rangarajan A, Behar KL, Shulman RG. Oxidative glucose metabolism in rat brain during single forepaw stimulation: a spatially localized ^{1}H[^{13}C]NMR study. *J. Cereb. Blood Flow Metab.* 1997; **17**: 1040–1047.
18. Hyder F, Petroff OAC, Mattson RH, Rothman DL. Localized ^{1}H NMR measurements of 2-pyrrolidinone in human brain in vivo. *Magn. Reson. Med.* 1999; **41**: 889–896.
19. Hyder F, Renken R, Rothman DL. In vivo carbon-edited detection with proton echo-planar spectroscopic imaging (ICED PEPSI): [3,4-$^{13}CH_2$]glutamate/glutamine tomography in rat brain. *Magn. Reson. Med.* 1999; **42**: 997–1003.
20. Hyder F, Brown P, Nixon TW, Behar KL. Mapping cerebral glutamate ^{13}C turnover and oxygen consumption by *in vivo* NMR in Oxygen transport to tissue XXI. (eds: Dunn JF and Swartz HM) Pabst, Lenerich, Germany, 2001.
21. Hyder F, Rothman DL, Blamire AM. Image reconstruction of sequentially sampled echo-planar data. *Magn. Reson. Imag.* 1995; **13**: 97–103.
22. Farzaneh F, Riederer SJ, Pelc NJ. Analysis of T_2 limitations and off-resonance effects on signal resolution and artifacts in echo-planar imaging. *Magn. Reson. Med.* 1990; **14**: 123–139.
23. Kida I, Hyder F, Kennan RP, Behar KL. Towards absolute quantitation of BOLD functional MRI. *Adv. Exp. Med. Biol.* 1999; **471**: 681–689.
24. Kida I, Kennan RP, Rothman DL, Behar KL, Hyder F. High-resolution CMR_{O2} mapping in rat cortex: a multi-parametric approach to calibration of BOLD image contrast at 7 Tesla. *J. Cereb. Blood Flow Metab.* 2000; **20**: 847–860.
25. Hyder F, Behar KL, Martin MA, Blamire AM, Shulman RG. Dynamic magnetic resonance imaging of the rat brain during forepaw stimulation. *J. Cereb. Blood Flow Metab.* 1994; **14**: 649–655.
26. Mosher TJ, Smith MB. Mapping the static magnetic field using a double-DANTE tagging sequence. *J. Magn. Reson.* 1991; **93**: 624–629.
27. Kennan RP, Scanley BE, Innis RB, Gore JC. Physiological basis for BOLD MR signal changes due to neuronal stimulation: Separation of blood volume and magnetic susceptibility effects. *Magn. Reson. Med.* 1998; **40**: 840–846.
28. Mandeville JB, Marota JJA, Kosofsky BE, Keltner JR, Weissleder R, Rosen BR, Weisskoff RM. Dynamic functional imaging of relative cerebral blood volume during rat forepaw stimulation. *Magn. Reson. Med.* 1998; **39**: 615–624.
29. Schwarzbauer C, Morrissey SP, Haase A. Quantitative magnetic resonance imaging of perfusion using magnetic labeling of water proton spins within the detection slice. *Magn. Reson. Med.* 1996; **35**: 540–546.
30. Calamante F, Thomas Dl, Pell GS, Wiersma J, Turner R. Measuring cerebral blood flow using magnetic resonance imaging techniques. *J. Cereb. Blood Flow Metab.* 1999; **19**: 701–735.
31. Mason GF, Rothman DL, Behar KL, Shulman RG. NMR determination of the TCA cycle rate and α-ketoglutarate/glutamate exchange rate in rat brain. *J. Cereb. Blood Flow Metab.* 1992; **12**: 434–447.
32. Mason GF, Gruetter R, Rothman DL, Behar KL, Shulman RG, Novotny EJ. Simultaneous determination of the rates of the TCA cycle, glucose utilization, α-ketoglutarate/glutamate exchange, and glutamine synthesis in human brain by NMR. *J. Cereb. Blood Flow Metab.* 1995; **15**: 12–25.
33. Shulman RG, Hyder F, Rothman DL. Cerebral energetics and the glycogen shunt: Neurochemical basis of functional imaging. *Proc. Natl Acad. Sci. USA* 2001; **98**: 6417–6422.
34. Grubb RL, Raichle ME, Eichling JO, Ter Pogosian MM. The effects of changes in pCO_2 on cerebral blood volume, blood flow, and vascular mean transit time. *Stroke* 1974; **5**: 630–639.
35. Kida I, Hyder F, Behar KL. Inhibition of voltage-dependent sodium channels suppresses the functional MRI response to forepaw somatosensory activation in the rodent. *J. Cereb. Blood Flow Metab.* 2001; **21**: 585–591.
36. Hyder F, Renken R, Kennan RP, Rothman DL. Quantitative multi-modal functional MRI with blood oxygenation level dependent exponential decays adjusted for flow attenuated inversion recovery (BOLDED AFFAIR). *Magn. Reson. Imag.* 2000; **18**: 227–235.
37. Rothman DL, Behar KL, Hetherington HP, den Hollander JA, Bendall MR, Petroff OA, Shulman RG. ^{1}H-observe/^{13}C-decouple spectroscopic measurements of lactate and glutamate in the rat brain *in vivo*. *Proc. Natl Acad. Sci. USA* 1985; **82**: 1633–1637.
38. Fitzpatrick SM, Hetherington HP, Behar KL, Shulman RG. The flux from glucose to glutamine in the rat brain *in vivo* as determined by ^{1}H-observed, ^{13}C-edited NMR spectroscopy. *J. Cereb. Blood Flow Metab.* 1990; **10**: 170–179.
39. Kuschinsky W, Paulson OB. Capillary circulation in the brain. *Cerebrovasc. Brain Metab. Rev.* 1992; **4**: 261–286.
40. Roy CS, Sherrington CS. On the regulation of the blood supply of the rat brain. *J. Physiol. (Lond.)* 1890; **11**: 85–108.
41. Hyder F, Kida I, Behar KL, Kennan RP, Rothman DL. Dominant events that modulate cortical oxygen diffusivity *in vivo* in Oxygen transport to tissue XXI. (eds: Dunn JF and Swartz HM) Pabst, Lengerich, Germany, 2001.
42. Ogawa S, Lee TM, Barrere B. The sensitive of magnetic resonance image signals of rat brain to changes in the cerebral venous blood oxygenation. *Magn. Reson. Med.* 1993; **29**: 205–210.
43. Prielmeier F, Nagatomo Y, Frahm J. Cerebral blood oxygenation in rat brain during hypoxic hypoxia. Quantitative MRI of effective transverse relaxation rates. *Magn. Reson. Med.* 1994; **31**: 678–681.
44. Hyder F, Shulman RG, Rothman DL. A model for the regulation of cerebral oxygen delivery. *J. Appl. Physiol.* 1998; **85**: 554–564.
45. Hyder F, Shulman RG, Rothman DL. Regulation of cerebral oxygen delivery. *Adv. Exp. Med. Biol.* 1999; **471**: 99–109.
46. Ueki M, Linn F, Hossman KA. Functional activation of cerebral blood flow and metabolism and after global ischemia of rat brain. *J. Cereb. Blood Flow Metab.* 1988; **8**: 486–494.
47. Crone C. The permeability of capillaries in various organs as determined by use of the "indicator diffusion" method. *Acta Physiol. Scand.* 1963; **58**: 292–305.
48. Siesjo BK. Brain Energy Metabolism. Wiley: New York, 1978.
49. Stewart GN. Researches on the circulation time in organs and on the influences which affect it: parts I–III. *J. Physiol. (Lond.)* 1894; **15**: 1–27.
50. Meier P, Zierler KL. On the theory of the indicator-dilution method for measurement of blood flow and volume. *J. Appl. Physiol.* 1954; **6**: 731–744.
51. Kvamme E, Torgner IA, Svenneby G. Glutaminase from mammalian tissues. *Meth. Enzymol.* 1985; **113**: 241–256.
52. Meister A. Glutamine synthetase from mammalian tissues. *Meth. Enzymol.* 1985; **113**: 185–199.
53. Van den Berg CJ, Garfinkel D. Simulation study of brain compartments—metabolism of glutamate and related substances in mouse brain. *Biochem. J.* 1971; **123**: 211–218.
54. Erecinska M, Silver IA. Metabolism and role of glutamate in mammalian brain. *Prog. Neurobiol.* 1990; **35**: 245–296.
55. Magistretti PJ, Pellerin L, Rothman DL, Shulman RG. Energy on demand. *Science* 1999; **283**: 496–497.
56. Schousboe A, Westergaard N, Sonnewald U, Petersen SB, Huang R, Peng L, Hertz L. Glutamate and glutamine metabolism and compartmentation in astrocytes. *Devl. Neurosci.* 1993; **15**: 359–366.
57. Sonnewald U, Westergaard N, Schousboe A, Svendsen JS, Unsgard G, Petersen SB. Direct demonstration by [^{13}C]NMR spectroscopy that glutamine from astrocytes is a precursor for GABA synthesis in neurons. *Neurochem. Int.* 1993; **22**: 19–29.

58. Maycox PR, Hell JW, Jahn R. Amino acid neurotransmission: spotlight on synaptic vesicles. *Trends Neurosci.* 1990; **13**: 83–87.
59. Peng L, Hertz L, Huang R, Sonnewald U, Petersen SB, Westergaard N, Larsson O, Schousboe A. Utilization of glutamine and of TCA cycle constituents as precursors for transmitter glutamate and GABA. *Devl. Neurosci.* 1993; **15**: 367–377.
60. Tsacopoulos M, Magistretti PJ. Metabolic coupling between glia and neurons. *J. Neurosci.* 1996; **16**: 877–885.
61. Rothstein JD, Martin L, Levey AI, Dykes-Hoberg M, Jin L, Wu D, Nash N, Kuncl RW. Localization of neuronal and glial glutamate transporters. *Neuron* 1994; **13**: 713–725.
62. Pellerin L, Magistretti PJ. Glutamate uptake into astrocytes stimulates aerobic glycolysis: a mechanism coupling neuronal activity to glucose utilization. *Proc. Natl. Acad. Sci. USA* 1994; **91**: 10625–10629.
63. Sokoloff L. Energetics of functional activation in neural tissues. *Neurochem. Res.* 1999; **24**: 321–329.
64. Hochachka PW. Mechanism and evolution of hypoxia-tolerance in humans. *J. Exp. Biol.* 1998; **201**: 1243–1254.
65. Moss GS, Dewoskin R, Rosen AL, Levine H, Palani CK. Transport of oxygen and carbon dioxide by hemoglobin-saline solution in the red-cell-free primate. *Surg. Gynecol. Obstet.* 1976; **142**: 357–362.
66. Homer LD, Weathersby PK, Kiesow LA. Oxygen gradients between red blood cells in the microcirculation. *Mircovasc. Res.* 1981; **22**: 308–232.
67. Klein B, Kuschinsky W, Schrock H, Vetterlein F. Interdependency of local capillary density, blood flow, and metabolism in rat brains. *Am. J. Physiol.* 1986; **251**: H1333–H1340.
68. Kleinfeld D, Mitra PP, Helmchen F, Denk W. Fluctuations and stimulus-induced changes in blood flow observed in individual capillaries in layers 2 through 4 of rat neocortex. *Proc. Natl Acad. Sci. USA* 1998; **95**: 15741–15746.
69. Vovenko E. Distribution of oxygen tension on the surface of arterioles, capillaries and venules of brain cortex and in tissue in normoxia: an experimental study on rats. *Pflügers Arch.* 1999; **437**: 617–623.
70. Kassissia IG, Goresky CA, Rose CP, Schwab AJ, Simard A, Huet PM. Tracer oxygen distribution is barrier-limited in cerebral microcirculation. *Circul. Res.* 1995; **77**: 1201–1211.
71. Davis TL, Kwong KK, Weisskoff RM, Rosen BR. Calibrated functional MRI: mapping the dynamics of oxidative metabolism. *Proc. Natl Acad. Sci. USA* 1998; **95**: 1834–1839.
72. Zhu XH, Kim SG, Andersen P, Ogawa S, Ugurbil K, Chen W. Simultaneous oxygenation and perfusion imaging study of functional activity in primary visual cortex at different visual stimulation frequency: Quantitative correlation between BOLD and CBF changes. *Magn. Reson. Med.* 1998; **40**: 703–711.
73. Silva AC, Lee SP, Yang G, Iadecola C, Kim SG. Simultaneous BOLD and CBF functional MRI during forepaw stimulation in rat. *J. Cereb. Blood Flow Metab.* 1999; **19**: 871–879.
74. Leach MJ, Marden CM, Miller AA. Pharmacological studies on lamotrigine, a novel potential antiepileptic drug: II. Neurochemical studies on the mechanism of action. *Epilepsia* 1986; **27**: 490–497.
75. Choi DW, Maulucci-Gedde M, Kriegstein AR. Glutamate neurotoxicity in cortical cell culture. *J. Neurosci.* 1987; **7**: 357–368.
76. Taylor CP, Narasimhan LS. Sodium channels and therapy of central nervous system diseases. *Adv. Pharmac.* 1997; **39**: 47–98.
77. Zhong J, Kennan RP, Fulbright RK, Gore JC. Quantification of intravascular and extravascular contributions to BOLD effects induced by alteration in oxygenation or intravascular contrast agents. *Magn. Reson. Med.* 1998; **40**: 526–536.
78. Greenberg JH, Sohn NW, Hand PJ. Nitric oxide and the cerebral blood flow response to somatosensory activation following deafferentation. *Exp. Brain Res.* 1999; **129**: 541–550.
79. Sokoloff L. Sites and mechanisms of function-related changes in energy metabolism in nervous system. *Devl. Neurosci.* 1993; **15**: 194–206.

